von Karman Institute for Fluid Dynamics

Lecture Series 1991-08

Laser Velocimetry

June 10 - 14, 1991

Review of Typical Applications
Wind Tunnels

James F. Meyers
NASA - Langley Research Center
Hampton, Virginia, USA

Review of Typical Applications
Wind Tunnels

by

James F. Meyers
NASA - Langley Research Center
Hampton, Virginia 23665
United States

Introduction

Laser velocimetry was first proposed in 1964 by Yeh and Cummins from Columbia University working under a grant from the National Science Foundation, reference 1. Their system was successfully tested in a low speed water flow. The next reported effort was by Forman, George, and Lewis from Brown Engineering, reference 2, who developed a system, under contract to NASA - Marshall Space Flight Center, designed to measure air flows. The technology was soon transferred to Marshall where Huffaker, Fuller, and Lawrence began to use the system in supersonic jets and wind tunnels, reference 3. Wind tunnel application of the technique began in earnest at the Arnold Engineering Development Center using a new dual-scatter technique (today known as the fringe-type laser velocimeter), references 4 and 5. The study of particle dynamics and their influence on flow field measurements in supersonic wind tunnels was investigated by Yanta, Gates, and Brown in 1971, reference 6. The first major international conference dedicated specifically to laser velocimetry and its applications was held at Purdue University, March 9-10, 1972, reference 7. Stevenson and Thompson provided a good forum for the exchange of research information. The conference was attended by the majority of scientists and engineers engaged in laser velocimetry research. Most of the 34 papers presented concentrated on the development of various aspects of the technique with only three papers addressing the application of laser velocimetry to wind tunnel flow fields. Two years later, a second conference was held at Purdue, reference 8. The 43 formal and 16 informal presentations show the increased interest in laser velocimetry. The increase to 17 papers addressing wind tunnel applications demonstrates the growing implementation of the technique to fluid mechanic investigations.

This lecture will address the use of laser velocimetry in wind tunnels. The applications include low speed flows in a miniature wind tunnel, investigation of a flow field with several techniques, large tunnels, and even a supersonic application. The intent is to illustrate the versatility of laser velocimetry to provide velocity information from the wide range

of flow fields developed in wind tunnels. The first investigation addressed will be the use of laser velocimetry to study a slow, but complicated flow field in a miniature wind tunnel.

Investigation of the Flow Within a Metalorganic Chemical Vapor Deposition Reactor

The metalorganic chemical vapor deposition process is widely used for production of electronic components, thin films and coatings, reference 9. The many variables involved in the process result in a complex dynamic system in which fluid dynamics, surface and gas-phase chemical reactions, temperature field, and external forces are all coupled. The physics involved in the flow field within the heated reactor are extremely complex and difficult to measure. The flow is extremely sensitive to small external effects such as temperature of the susceptor, chemical composition, and even gravity. Therefore probe techniques can not be used to measure the flow physics. Even if the presence of a probe would not affect the flow, the corrosive nature of the fluid would soon destroy it. Therefore a laser velocimeter is an ideal technique to characterize the operation of particular reactors. Investigation of the underlying physics as well as the effects of operating conditions will provide the information necessary to design reactors based on sound fluid mechanics instead of the trial-and-error methods used today.

The Chemical Vapor Deposition Facility was created at NASA - Langley Research Center by Johnson, Hyer, Culotta, Black, Clark, and Timmons, reference 10, to enhance scientific understanding of the reactive fluid dynamics of chemical vapor deposition. The facility is designed to be capable of investigating the fluid flow in vertical or horizontal reactors up to 0.5 m in diameter, with either cold or radio frequency (RF) heated flows. A key element in the facility is the orthogonal three component laser velocimeter, figure 1. This system uses orthogonal collection of scattered light to reduce the sample volume to a 150 micron sphere and to reduce collected flare from surfaces. The optical components can be easily configured to measure the flow in any test reactor, even through hand blown glass surrounded by an RF coil heater.

An example reactor investigated in reference 10 was designed to operate in a horizontal cylindrical tube configuration, figure 2. Instead of the usual hemispherical inlet section, a flat, elliptical plate was welded to the circular cylinder at 31° to the axis of the cylinder. The inlet tube for the gas supply was blended into the joint at the bottom of the cylinder and aligned with the major axis of the elliptical plate. The growth region on the face of the graphite susceptor was also slanted at 31° to the

cylinder axis, thus forming a uniform gap between the susceptor and the front face.

The primary purposes of this example investigation were to characterize the fluid mechanics of the reactor and examine the effects of buoyancy-induced convection. The independent variable investigated was the temperature. An optimum set of operating conditions for this reactor was not known a priori. The baseline data set was first obtained by measuring the flow velocities at room temperature with the input flow rate of 3 l/min. The nitrogen gas flow was seeded with 1.3 micron polystyrene particles. The cold reactor data obtained in a plane 6.2 mm from the susceptor surface are presented in figure 3. The susceptor was then brought to a typical growth temperature for GaAs of 700° C by RF induction heating of the graphite susceptor. The resulting measurements are presented in figure 4.

The laser velocimeter measurements clearly show the effects of buoyancy-induced convection when the susceptor is heated. Thermal convection is the dominate factor in the fluid dynamics of the reactor at growth temperatures. Heating of the susceptor increased gas velocities inside the reactor by as much as a factor of five.

Helicopter Flow Field Investigations in the 4x7-meter Low Speed Wind Tunnel

Since the first application was in a miniature wind tunnel, it is appropriate to look next at the tunnel with the largest multi-component laser velocimeter in the world. The 4x7-meter Low Speed Wind Tunnel is the premier NASA test facility for the investigation of helicopter fluid dynamics. The physical size of powered helicopter models requires the laser velocimeter to measure the velocity within a volume 2 m on a side located along the centerline of the test section. The streamwise and vertical laser velocimeter components are placed on a large traversing mechanism capable of moving the measurement volume within a plane 2 m on a side. The cross tunnel traverse is accomplished using a 0.3 m diameter zoom lens capable of focusing the laser beams from 3 m to 8 m. A pan/tilt mirror is placed just following the zoom lens to allow the sample volume to be aligned parallel with the rotor blades at a desired rotor azimuth. Velocity measurements are made from 1.7 micron polystyrene particles. The system is described in reference 11 and shown in figures 5 and 6.

The advancement of predictive computer models of the rotor flow field has created a need for detailed experimental verification data. This data must be fully three dimensional and include higher statistical

moments such as turbulence intensity and Reynolds stress. A review of three dimensional laser velocimetry techniques by Meyers, reference 12, indicates that the only method with the required accuracy is an orthogonal configuration. Thus a single component system using a third color from the Argon ion laser is currently under construction, figure 7. The system is placed on a flattened four degree of freedom traversing mechanism with an aerodynamic shell on the floor of the test section. It is anticipated that this structure, 0.3 m high, will not disturb the flow field about the rotor located 2.0 m above. This traversing mechanism will be computer controlled to track the motions of the other system to maintain overlap of the two measurement volumes.

The flow field about a helicopter rotor is extremely complicated. It is known that the performance of the rotor is affected by the interaction of a trailing blade with the air flow generated by the previous blade. The extent of this interaction and its affect on the total flow field is virtually unknown. An attempt to begin understanding this interaction was to measure the flow entering the rotor disk. If the rotor induced changes to the inlet flow, the angle-of-attack and thus the loading on each blade would vary based on these changes.

The baseline investigation was to measure the average steady state velocity field one blade chord above the rotor disk. Theoretical predictions of this flow as described by Hoad, Elliott and Althoff, reference 13, indicated the vertical velocity component should be slightly positive at the leading edge of the disk and strongly negative at the trailing edge. The predictions also indicate the flow is symmetrical about the centerline of the model.

The following investigation conducted by Elliott, Althoff and Sailey, reference 14, used conditional sampling to measure the velocity field as a function of rotor azimuth. Two auxiliary channels in the data acquisition subsystem, reference 15, were triggered by the streamwise and vertical component channels to read the rotor shaft encoder when their respective velocity channel made a measurement. Thus the final data ensemble can be interrogated and velocity measurements obtained for a given rotor azimuth to determine the velocity statistics. Examples of the results are illustrated in figures 8, 9, 10, 11, and 12 for azimuth angles of 0.0°, 22.5°, 45.0°, 67.5° and 90.0° respectively. If the velocity vectors and flow angles are desired, coincidence (both components must obtain a measurement within the particle transit time across the sample volume) can be imposed by summing the measured interarrival times in each component and selecting measurements where the two sums match.

The experimental results clearly show asymmetries with large velocity gradients on the advancing side of the disk. There is also a dependence of the inlet flow field on rotor azimuth indicating an influence of blade location upstream. The differences between azimuth angles of 0°, figure 8, and 90°, figure 12, is attributed to slight variations in the path of individual rotor blades as they circulate.

Boundary Layer Measurements in a Supersonic Flow Using a Laser Transit Anemometer

Examples of laser velocimeter applications in extremes of facility size have been described, now it is time to move to a fast facility. A demonstration of laser velocimetry capabilities was conducted in the Langley Unitary Plan Wind Tunnel by Humphreys, Hunter, Covell and Nichols, reference 16. The wind tunnel is a closed-circuit, continuous-flow pressure tunnel with two 1.22-x 1.22-meter test sections. The tunnel is designed to operate at pressure from near vacuum to 10 atm. The free stream Mach number can be adjusted from 2.30 to 4.63 using a nozzle with an asymmetric sliding-block. The unit Reynolds number thus varies from 1.64×10^{6} to 26.23×10^{6} /m. The demonstration experiment was to probe the boundary layer of a slender, 5° half-angle, cone model using a laser transit anemometer. The wind tunnel is shown with the laser transit anemometer positioned at the side of the test section in figure 13.

The laser transit anemometer uses a Wollaston prism to split the incoming laser beam into two parallel beams. The beams are sent through a dove prism to provide rotation of the two beams in the sample volume to align the measurement direction with the primary flow direction. The signals obtained as a particle passes through each beam are collected and routed using fiber optics to separate photomultipliers. The output pulse from each photomultiplier is passed to an electronic signal correlator to compute the cross correlation. The location in time of the peak in the correlogram is the most likely travel time for a particle to pass between the two laser beams, and thus the inverse of the mean flow velocity.

The model, diagramed in figure 14, had a 5° half angle cone forebody, a cylindrical midbody, and a 9° truncated cone afterbody. The boundary layer was seeded using 0.9 micron aluminum silicate particles. The particles, aerated using a small vibrating fluidized bed, were injected through nine 1.32 mm orifices located as a grid at x/L of 0.25 on the model forebody. The boundary layer profiles were measured at x/L of 0.7 above the model forebody just upstream of the cylindrical midbody.

Vertical profiles were measured in a plane bisecting the model's longitudinal centerline with the model positioned at 0° angle-of-attack.

The boundary layer flow was assumed to be parallel to the model surface, thus the laser beams were oriented accordingly and only a single velocity correlogram was collected at each measurement point. The boundary layer was interrogated with the freestream Mach number set to 2.5 and 4.5. These two surveys, shown in figures 15 and 16 respectively, are compared with theoretical laminar and turbulent boundary layer profiles. The measurements with the freestream Mach number of 2.5 compare well with the predicted profile for a turbulent boundary layer. However, measurements on a similar cone by Fisher and Dougherly, reference 17, indicate the transition to turbulence should occur at a higher Reynolds number than the present investigation. This early transition may be due to the ejection of the seeding particles from the grid of orifices. Shadowgraph photographs reported in reference 16 clearly show shocks emanating from the grid. The measurements deviate from theory with the Mach number set to 4.5, possibly from increased model vibration. As the model moves, the velocity within the boundary layer is time averaged by the laser transit anemometer increasing the width of the measured velocity correlogram and thus decreasing the accuracy of mean velocity estimates.

The Basic Aerodynamic Research Tunnel

Instead of continuing to describe laser velocimeter applications in various tunnels, the lecture will now concentrate on a specific facility, the Basic Aerodynamic Research Tunnel, reference 18. It was designed to be a stable platform for the detailed investigation of fundamental aerodynamic flow fields. Its primary function is to provide the experimental data necessary for the development and verification of generalized computational fluid dynamic computer codes. It is also an excellent facility for the development of advanced instrumentation. The facility, shown in figure 17, is an open circuit tunnel that has a test section measuring 0.71 m high, 1.02 m wide and 3.05 m long. The test section is divided into two 1.524 m long bays. The maximum flow velocity in the test section is 67 m/sec which yields a Reynolds number of 4.6×10^{6} /m. The airflow entering the test section is conditioned by a honeycomb, four anti-turbulence screens and an 11:1 contraction ratio. The 0.1 m thick honeycomb has a 0.01 m cell size. The screens are 7.87 mesh per centimeter with a porosity (ratio of open area to total area) of 64 percent. These flow conditioners coupled with an excellent fan speed controller, provide a low-turbulence, uniform flow in the test section. The variation in the longitudinal component of turbulence intensity (measured with a hot wire) with test section q is from

approximately 0.05 percent at q = 4.13 N/m^2 (V_∞ = 28 m/sec) to 0.08 percent at q = 18.6 N/m^2 (V_∞ = 59.4 m/sec).

In keeping with the primary function of the facility, measurements of the vortical flow field above a 75° delta wing and a YF-17 model were made with an orthogonal three component fringe type laser velocimeter. The capabilities of the facility for instrumentation development are illustrated by proof-of-concept investigations using a particle image velocimeter to measure the flow about a NACA-0012 airfoil and a Doppler global velocimeter to measure the vortical flow above the 75° delta wing.

Vortical Flow Above a 75° Delta Wing

The subject of the investigation by Meyers and Hepner, reference 19 is the flow above a 75° delta wing. The low turbulence input flow of the Basic Aerodynamics Research Tunnel remains stable for the long periods of time required to conduct detailed investigations. The model is a 75° swept delta wing with a 0.305 m span and sharp leading edges (10° bevel on the lower surface with the upper surface flat). An angle-of-attack of 20.5° yields a stable vortex flow above the model. An increase of angle-of-attack to 40.0° yields burst vortices. The tunnel speed is adjusted to obtain a chord Reynolds number of 1.0 million (q = 8.4 N/m^2) for both conditions. The velocity flow field investigations were conducted in a plane orthogonal to the surface of the model at an x/L = 0.7.

The laser velocimeter is an orthogonal three component system with color separation. The Argon ion laser wavelengths, 496.5 nm, 476.5 nm and 514.5 nm are chosen for the U (streamwise), V (vertical), and W (traverse) components respectively. The transmission optical system for the U and V components is located on the side of the test section with the receiving optical system located above the test section slightly off-perpendicular (15°) toward the upstream direction. The transmission optical system for the W component is placed above the test section perpendicular to the U-V optical axis. Its receiving optical system is adjacent to the U-V transmitter, rotated 15° downstream about the sample volume. This configuration yields a very small spherical sample volume, 140 microns in diameter, and reduces the amount of scattered light or flare from the model surface entering the collecting optical system. The sample volume can be placed within 70 microns from the unprepared model surface before flare reduces signal-to-noise below acceptable limits for the signal processing instrumentation. All three optical components contain Bragg cells to provide full measurement directionality.

The optical system and Argon ion laser are placed on a three component mechanical traversing system. The traversing mechanism surrounds the test section providing the maximum number of optical mounting locations for flexibility of optical configuration designs for future test requirements. The mechanism provides a traversing range of one cubic meter with a resolution of 0.01 mm in each axis. The optical system and laser move as a unit driven by two slaved stepper motors in each of the two horizontal directions and by four slaved stepper motors in the vertical direction. The laser velocimeter mounted on the traversing mechanism is shown installed around the test section in figure 18.

The flow above the delta wing with an angle-of-attack of 20.5° consists of two stable leading edge vortices. A laser light sheet visualization of these vortices is shown in figure 19. In reference 18, Sellers and Kjelgaard studied this flow field using surface and laser light sheet visualizations, Pitot pressure surveys, and 5-hole probe surveys. Theoretical estimates of the flow were computed using the CFL3D code, reference 20, which uses a thin-layer formulation of the Navier-Stokes equations. The experimental and theoretical results compared well with the laser velocimeter data in regions of low velocity gradients, but deviated near the core to differences of up to 35 percent. The laser velocimeter was the only technique that could obtain turbulence results and descriptions of the velocity flow field when the angle-of-attack was increased to 40.0°, bursting the vortices.

The three component mean velocity measurements obtained with the laser velocimeter at an angle-of-attack of 20.5° are shown in figure 20 and at 40.0° in figure 21. It is noted that the streamwise component increases to twice freestream velocity within the core of the vortex, but reverses when the vortices burst. The angular motion seems to change little in either case. The measurements of flow turbulence intensity are presented for the streamwise component, figures 22 and 23, the vertical component, figures 24 and 25, and the traverse component, figures 26 and 27. The streamwise component contains the maximum turbulence near the core of the vortices while the maximum for the other two components are outboard of the vortices.

Vortical Flow Above a YF-17 Model

The flow field measurements above the delta wing were part of an investigation to provide general knowledge about vortex flow fields and establish a measurement database for verification of computational fluid dynamics computer code. This investigation also served as a preliminary test to determine the performance of the laser velocimeter when measuring vortex flows. The final goal of the program conducted

by Sellers, Meyers and Hepner, reference 21, was to investigate the flow above a YF-17 model to determine the vortex interaction with the vertical stabilizers.

Modern fighter aircraft at high angles of attack generate vortices which produce substantial increases in lift. The vortices are shed by the sharp wing leading edges, slender fuselage forebodies, and by the highly-swept wing leading-edge extensions (LEXs). There is also interest in techniques which exploit the vortices to provide increases in maneuverability in the high-alpha regime where conventional control surfaces lose their effectiveness, reference 22. Figure 28 is a photograph of an F-18 aircraft at high angle-of-attack and shows the LEX vortices made visible with a smoke bomb.

The interaction of the vortices with the tail surfaces can cause structural problems. Both the F-15, reference 23 and the F-18, reference 24, have encountered buffeting and/or structural fatigue problems with the vertical tails at high angles of attack. The buffeting is due in a large part to the breakdown of the vortices ahead of the tails. Vortex bursting or breakdown is meant to describe the condition where the axial velocity at the core of the vortex abruptly stagnates followed by a rapid expansion of the vortex core. After the expansion, the flow changes to a highly-turbulent swirling state.

The lack of quantitative flow field data has hampered efforts to develop theoretical methods to predict aircraft buffet or a buffet design criteria for the high angle-of-attack flight regime. There have been numerous research papers written on the subject of vortex flows from slender delta wings, but much of this data is of limited use, since the instrumentation that was available at the time was not capable of measuring the velocity field in a burst vortex. Flow field data above configurations are even more scarce.

The model was a Northrop YF-17 configuration which was the prototype for the McDonnell Douglas F/A-18 Hornet. The YF-17 shown in the three-view sketch in figure 29 incorporates design features that are typical of many of the current generation fighter aircraft. It includes a moderately-swept (26.6°) wing, twin vertical tails, and a highly-swept (80°) leading edge extension. The flow field generated by this aircraft exhibits many of the characteristics of the present generation fighter aircraft, as well as the problems such as vortex interaction with the tail surfaces.

All data were obtained at a free stream dynamic pressure of 30 lb/ft^2, which represents free stream velocities of 159 ft/sec. This speed results in test Reynolds numbers of 326,000 based on the mean aerodynamic

chord. The two angles of attack, 15° and 25°, investigated represented conditions where the vortices over the model would be unburst and burst, respectively. The higher angle-of-attack represented a condition where, based on Northrop YF-17 flight test data, the tail buffet loads increase significantly. The two survey stations, 440 and 524, where flow field data were obtained are shown in figure 29. Velocity measurements were acquired over the right half of the model.

The laser velocimeter mean velocity measurements are shown as contour maps of streamwise velocity and vectors for the velocities within the plane normal to freestream. The results for stations 440 and 524 are shown in figures 30 and 31 respectively for an angle-of-attack of 15°. The cross flow vectors clearly show the LEX vortex is positioned outboard of the vertical tail and close to the wing upper surface. The spanwise component of velocity has accelerated to approximately 90 percent of freestream directly under the LEX vortex. The streamwise component of velocity in the core of the LEX vortex has decelerated to approximately 80 percent of freestream. The flow separates at the leading edge of the wing at this angle-of-attack. There is a large separated flow region over the outer wing panel at these stations. There are reversed flows of up to 10 percent of freestream in the streamwise velocity component over the outer third of the wing span. The LEX vortex had the favorable effect of preventing wing separation over the inboard portion of the wing.

The flow field takes on a dramatically different character at 25° angle-of-attack. The mean velocity vectors and contours are shown in figures 32 and 33 for stations 440 and 524 respectively. The cross flow velocity vectors show that the wing separation region and the LEX vortex have grown in size and the LEX vortex is positioned directly in line with the vertical tail. The LEX vortex has burst at the 440 station at this angle-of-attack. The core of the LEX vortex magnifies at the 524 station and contains a large area of reversed flow as shown in figure 33. The reversed flow reaches a maximum of approximately 10 percent of freestream. Although the LEX vortex has burst, there is still a structured swirling pattern around the vortex. This is consistent with the measurements of a burst vortex over the 75° delta wing, figure 21, however the flow field is more complicated due to the presence of the wing separation which has merged with the flow from the LEX vortex. The region of reverse flow in the wing separation region has grown in both size and strength with the magnitude of the reverse flow increasing to approximately 20 percent of freestream.

The standard deviation of velocity provides a measure of the intensity of the fluctuating input forcing the vertical tail to vibrate. The standard deviation is nondimensionalized by the freestream velocity to provide a

measure of the relative turbulence intensity. The normalized standard deviation for the streamwise, vertical and spanwise components are shown in figures 34, 35, and 36 respectively for the 524 station at an angle-of-attack of 25°. The maximum value for the normalized standard deviation reaches levels of approximately 0.40, 0.35, and 0.30 for the streamwise, vertical and spanwise components respectively. Along with being large values, the regions of influence are quite large. The large standard deviations in the upper portion of the wing separation region are due to movement of the shear layer through the measurement location.

Particle Image Velocimetry Measurements of the Flow About a NACA 0012 Airfoil

The use of the Basic Aerodynamic Research Tunnel as a test facility for the development of advanced instrumentation systems is demonstrated by performing a proof-of-concept test of the particle image velocimeter (PIV). Although particle image velocimetry is simple in concept, reference 25, the analysis of the double exposed photographs is far from simple. Traditionally the analysis is performed in the Fourier plane with such techniques as Young's fringe analysis and / or 2-D spatial correlation. These approaches require heavy seeding to obtain sufficient particle pairs needed to delineate a clear peak in the Fourier plane. They are also computationally intensive, and unless special and typically expensive computing platforms are utilized, the computation of the Young's fringe images and / or correlations over a photograph can be a slow process. For these reasons a new analysis technique, performed totally in the image plane, has been developed by Humphreys, reference 26, which rapidly extracts all available vectors from the photograph without the need for heavy seeding nor extensive computations.

The demonstration of PIV and the new analysis technique was to map the flow field over a NACA 0012 airfoil at a 5° angle-of-attack and a freestream velocity of 45 m/sec. The test used 0.8 micron polystyrene particles as scattering centers. A diagram illustrating the PIV concept is shown in figure 37 and the data acquisition optical system in figure 38. A photograph of the optical system mounted to the laser velocimeter traversing mechanism is shown in figure 39.

The photograph optical analysis system consists of a film holder mounted on a traversing mechanism, an illumination source, and a viewing CCD camera. White light illumination is used to eliminate the problem of unwanted fringe patterns from supporting glass plates normally encountered in the traditional approach using lasers. A zoom

lens is used to vary the field of view of the camera to obtain the desired interrogation region.

The video image of an interrogation region is analyzed to determine the centroid of each particle image. Once the centroid map is obtained, the extraction of vectors begins by centering on each centroid, one by one in the map, a circular neighborhood with radial bounds of 20 percent of the interrogation region length. Within each neighborhood, all possible pairings are formed between the test centroid at the center of the neighborhood and any other centroids falling in the radial bounds. The neighborhood / pairing process is repeated for each centroid occurring in the map, generating an ensemble of all possible vectors corresponding to the various pairings. For any particular neighborhood only one correct pairing can be formed; however, any number of false pairings can occur. Once the completed ensemble of vectors from the centroid map is formed, valid vectors are identified through the use of magnitude and angle histograms which are formed from the ensemble. Each histogram is set to 10 bins which can be sparse because the majority of centroid maps contain relatively few entries. Even when sparse, a definite peak will be exhibited, corresponding to the most frequently occurring magnitude and angle in the ensemble and thus in the interrogation region. If an ambiguity exists in one of the two histograms due to two or more equal height peaks being present, then the other histogram takes precedence. If an ambiguity exists in both histograms, then the interrogation region is undefined and is rejected. The final step in the processing is to select from the ensemble only those vectors matching the most frequently occurring vector as identified by the histogram peaks.

Once the vector field has been generated for the entire photograph, adjacent vectors are compared to reject those vectors which differ widely from their neighbors. The validated vectors are then projected onto a uniform grid using weighted averages based on distance from the desired grid point. The average vector field is then visually inspected to remove any further erroneous vectors remaining in the field.

A typical photograph of the flow field about the NACA 0012 airfoil was interrogated with the interrogation region set to obtain between 3 and 5 centroid pairs with an average displacement of 20 percent of the interrogation region size. The false vector rate exhibited during the analysis was approximately 5 percent which compares favorably to rates predicted by the simulation study conducted in reference 26. The 2,500 interrogation regions investigated on the film required approximately 3 hours of processing time using a Micro VAX II minicomputer. This compares favorably with the traditional approach using Fourier

transforms computed using a 33 MFLOP array processor. The resulting flow field map is shown in figure 40.

Vortical Flow Above a 75° Delta Wing Measured with Doppler Global Velocimetry

Continuing with instrument development in the Basic Aerodynamic Research Tunnel, another global velocity measuring technique is currently undergoing development. In the manner of particle image velocimetry, the Doppler global velocimeter, DGV, uses a laser light sheet to illuminate a particle field within the flow to simultaneously make multiple velocity measurements, reference 27. However, instead of measuring the time-of-flight between multiple exposures of the particle field, the DGV measures the Doppler shift of light scattered from the illuminated particles. This approach improves on PIV by providing the capability to measure the full three component velocity field without directional ambiguity.

The velocity component measured is determined by the placement of the laser light sheet and the receiving optical system. If the propagation direction of the laser light sheet is represented by the unit vector $\hat{i}$, and the propagation direction of the collected scattered light represented by the unit vector $\hat{o}$, the velocity component measured is parallel to the difference between these two unit vectors, $\hat{o} - \hat{i}$. As shown in figure 41, the measured velocity vector, $\hat{o} - \hat{i}$, is the vector perpendicular to the bisector of vectors $\hat{o}$ and $\hat{i}$ lying within the plane defined by the vectors $\hat{o}$ and $\hat{i}$. Thus for a general flow velocity vector $\mathbf{V}$, the shift in frequency, $\Delta\upsilon$, of the collected scattered laser light is dependent on the vectorial dot product between the velocity vector $\mathbf{V}$ and the measurement vector $\hat{o} - \hat{i}$ as shown in equation 1:

$$\Delta\nu = \frac{\nu_o\,(\hat{o} - \hat{i}) \bullet \mathbf{V}}{c} \qquad (1)$$

where ν_o is the optical frequency of the laser light sheet and c is the speed of light. Three component measurements are possible by selecting three observation directions, $\hat{o}_1$, $\hat{o}_2$, and $\hat{o}_3$, or selecting three propagation directions of the laser light sheet, $\hat{i}_1$, $\hat{i}_2$, and $\hat{i}_3$.

Classic approaches to measure the Doppler shift of the scattered light use heterodyne detection to mix shifted scattered light with unshifted reference light to obtain the difference (Doppler) frequency. Instead, Doppler global velocimetry uses the edge of an absorption line in molecular Iodine to serve as a frequency discriminator to directly measure the Doppler shift of the collected scattered light, reference 27.

An Argon ion laser operating in single line mode at 514.5 nm is tuned by tilting the intercavity etalon to an optical frequency corresponding to a point midway along the edge of an absorption line of an Iodine absorption line filter (ALF), figure 42. Collected scattered light from a stationary object or cloud of particles will be attenuated by 50 percent as it passes through the ALF. If the object or particle cloud is moving, the attenuation through the ALF will increase (or decrease depending on the direction of movement) by an amount proportional to the Doppler shift. By using the ALF as a filter for a CCD camera, an entire laser light sheet can be viewed and the velocity field determined.

In practice, particle size distribution and number density, and the laser light sheet intensity profile are other factors influencing the amount of collected scattered light reaching the viewing camera. These influences can be minimized by viewing the same scene with a second camera without an ALF, figure 43, to provide a reference signal used to normalize the viewing camera output. The two cameras must be aligned with corresponding pixels in each camera viewing the same portions of the light sheet. Other influences from nonuniform optical elements and variations in pixel sensitivities in the CCD cameras are removed using pixel-by-pixel ratio calibrations.

The stability of the flow field in the Basic Aerodynamic Research Tunnel and the multiple investigations of the flow field above the 75° delta wing make this an ideal proof-of-concept for the Doppler global velocimeter, reference 28. Again the delta wing was set to an angle-of-attack of 20.5° to obtain a stable vortical flow field. The DGV was placed in the wind tunnel with the illuminating light sheet oriented normal to the streamwise direction passing through the side of the tunnel. The receiver was placed in forward scatter, 53 degrees out of plane from the light sheet as seen in figure 44. This provided a measurement velocity vector in the horizontal plane, 26.5° from the streamwise direction. The flow was seeded using the propylene glycol vaporization/condensation generator normally used for flow visualization. The data acquisition consisted of capturing simultaneous frames from the signal and reference cameras with the digital dual frame grabber. The frame grabber normalizes the signal camera output pixel-by-pixel with the reference image and then transfers the resulting image to the controlling computer for pseudo color mapping and data storage. A typical image of the vortex flow field is shown in figure 45 where the dark regions indicate slower velocities. If the amplitude of the normalized image along a line through the center of the vortices is plotted, figure 46, the increased velocity (lower amplitude) toward the vortex core is clearly seen. The amplitude variations in the signal and reference images are seen be removed through the normalization process. The normalized images can be used to obtain flow statistics

similar to other techniques except the entire flow field is investigated simultaneously. Low frequency time dependent flows can also be investigated in a global sense.

What is the Future of Wind Tunnel Testing with Laser Velocimetry

The several laser velocimetry applications presented illustrate the versatility of the technique for wind tunnel testing. The techniques can be divided into two classifications: point measurement techniques with excellent measurement accuracy, and global techniques that can measure the entire velocity flow field within a plane simultaneously but with lower accuracy. Future wind tunnel investigations will incorporate both classifications in aerodynamic testing. Global techniques will be incorporated to quickly determine the general characteristics of the flow including monitoring the effects of changes in the test conditions such as changing the model angle of attack. They can also be used to monitor time dependent flow conditions. Using global techniques in this manner will greatly decrease the tunnel time required to describe the flow field. However, reviewing the results of the global investigation will probably reveal portions of the flow field where detailed measurements are required. These are the areas where point measurement techniques will make their contribution.

Testing flows in this manner will result in the acquisition of experimental data at a rate and quality comparable with results from computational fluid dynamics computer codes. This will result in a closer coupling between theory and experiment. Using this approach, designers of the next generation of aircraft will be equipped with the knowledge necessary to increase the efficiency and performance of the resulting aircraft.

References

1. Yeh, Y.; and Cummins, H. Z.: *Localized Fluid Flow Measurements with an He-Ne Laser Spectrometer*. Applied Physics Letters, Vol. 4, No. 10, May 1964, pp. 176-178.

2. Foreman, J. W., Jr.; George, E. W.; and Lewis, R. D.: *Measurement of Localized Flow Velocities in Gases with a Laser Doppler Flowmeter*. Applied Physics Letters, Vol. 7, No. 4., August 15, 1965, pp. 77-78.

3. Huffaker, R. M.; Fuller, C. E.; and Lawrence, T. R.: *Application of Laser Doppler Velocity Instrumentation to the Measurement of Jet Turbulence*. Society of Automotive Engineers, paper 690266, January, 1969.

4. Lennert, A. E.; Brayton, D. B.; Goethert, W. H.; and Smith, F. H.: *Laser Applications for Flow Field Diagnostics.* Laser Journal, Vol. 2, No. 2, March/April, 1970, pp. 19-27.

5. Lennert, A. E.; Brayton, D. B.; Crosswy, F. L.; *et. al.*: *Summary Report of the Development of a Laser Velocimeter to be Used in AEDC Wind Tunnels*. AEDC-TR-70-101, U.S. Air Force, July 1970.

6. Yanta, W. J.; Gates, D. F.; and Brown, F. W.: *The Use of a Laser Doppler Velocimeter in Supersonic Flow*. AIAA paper 71-287, AIAA 6th Aerodynamic Testing Conference, March 10-12, 1971.

7. Stevenson, W. H.; and Thompson, H. D. - Editors: **Proceedings of the Project Squid Workshop on the Use of the Laser Doppler Velocimeter for Flow Measurements**. Purdue University, March 9-10, 1972.

8. Stevenson, W. H.; and Thompson, H. D. - Editors: **Proceedings of the Project Squid Workshop on the Use of the Laser Velocimeter for Flow Measurements**. Purdue University, March 27-29, 1974.

9. Sherman, A.: **Chemical Vapor Deposition for Microelectronics: Principles, Technology, and Applications**. Noyes, Park Ridge, NJ, 1987.

10. Johnson, E. J.; Hyer, P. V.; Culotta, P. W.; Black, L. R.; Clark, I. O.; and Timmons, M. L.: *Characterization of MOCVD Fluid Dynamics by Laser Velocimetry*. Journal of Crystal Growth, 109 (1991) North-Holland, pp. 24-30.

11. Meyers, J. F.: *Analysis of the Dedicated Laser Velocimeter Systems at NASA - Langley Research Center*. Proceedings of the Fourth International Symposium on Applications of Laser Anemometry to Fluid Mechanics, Lisbon, Portugal, paper 12.4, July 11-14, 1988.

12. Meyers, J. F.: *The Elusive Third Component.* Proceedings of the International Symposium on Laser Anemometry. 1985 Winter Annual Meeting, ASME Fluids Engineering Division, Miami, FL, November 17-22, 1985, pp. 247-254.

13. Hoad, D. R.; Elliott, J. W.; and Althoff, S. L.: *Rotor Inflow Variability with Advance Ratio*. 44th Annual Forum of the American Helicopter Society, Washington, DC, 1988.

14. Elliott, J. W.; Althoff, S. L.; and Sailey, R. H.: *Inflow Measurements Made With a Laser Velocimeter on a Helicopter Model in Forward Flight, Volume III Rectangular Planform Blades at an Advance Ratio of 0.30*. NASA TM-100543, 1988.

15. Cavone, A. A.; Sterlina, P. S.; Clemmons, J. I., Jr.; and Meyers, J. F.: *A High-Speed Buffer for LV Data Acquisition*. Proceedings of the International Congress on Instrumentation in Aerospace Simulation Facilities, College of William and Mary, Williamsburg, VA, pp. 113-119.

16. Humphreys, W. M., Jr.; Hunter, W. W., Jr.; Covell, P. F.; and Nichols, C. E., Jr.: *Laser Transit Anemometer Measurements on a Slender Cone in the Langley Unitary Plan Wind Tunnel*. NASA TM–102775, December 1990.

17. Fisher, D. F.; and Dougherty, N. S.: *Flight and Wind Tunnel Correlation of Boundary Layer Transition on the AEDC Transition Cone*. AGARD-CP-339, 1982.

18. Sellers, W. L., III; and Kjelgaard, S. O.: *The Basic Aerodynamics Research Tunnel - A Facility Dedicated to Code Validation*. AIAA 15th Aerodynamic Testing Conference, San Diego, California, paper AIAA-88-1997, May 18-20, 1988.

19. Meyers, J. F.; and Hepner, T. E.: *Measurement of Leading Edge Vortices from a Delta Wing Using a Three Component Laser Velocimeter*. AIAA 15th Aerodynamic Testing Conference, San Diego, California, paper AIAA-88-2024, May 18-20, 1988.

20. Thomas, J. L.; Taylor, S. L.; and Anderson, W. K.: *Navier-Stokes Computations of Vortical Flows Over Low Aspect Ratio Wings*. AIAA paper 86-0207, January, 1987.

21. Sellers, W. L., III; Meyers, J. F.; and Hepner, T. E.: *LDV Surveys over a Fighter Model at Moderate to High Angles of Attack*. SAE 1988 Aerospace Technology Conference & Exposition, Anaheim, California, October 3-6, 1988.

22. Murri, D. G.; and Rao, D. M.: *Exploratory Studies of Actuated Forebody Strakes for Yaw Control at High Angles of Attack*.

AIAA–87-2557, AIAA Atmospheric Flight Mechanics Conference, Monterey, California, August 1987.

23. Triplett, W. E.: *Pressure Measurements on Twin Vertical Tails in Buffeting Flow*. Journal of Aircraft, Vol. 20, No. 11, November 1983.

24. Wentz, W. H., Jr.: *Vortex-Fin Interaction on a Fighter Aircraft*. AIAA-87-2474, AIAA 5th Applied Aerodynamics Conference, Monterey, California, August 1987.

25. Adrian, R. J.: *Processing Techniques: Image Plane and Fourier Plane*. von Karman Lecture Series 1988-06, Particle Image Displacement Velocimetry, 1988.

26. Humphreys, W. M., Jr.: *A Histogram-Based Technique for Rapid Vector Extraction from PIV Photographs*. Proceedings of the Fourth International Conference on Laser Anemometry - Advances and Applications, Cleveland, Ohio, August 5-9, 1991.

27. Komine, H.; Brosnan, S. J.; Litton, A. B.; and Stappaerts, E. A.: *Real-Time Doppler Global Velocimetry*. AIAA 29th Aerospace Sciences Meeting, Reno, Nevada, paper no AIAA-91-0337, January 7-10, 1991.

28. Meyers, J. F.; and Komine, H.: *Doppler Global Velocimetry - A New Way to Look at Velocity*. Proceedings of the Fourth International Conference on Laser Anemometry - Advances and Applications, Cleveland, Ohio, August 5-9, 1991.

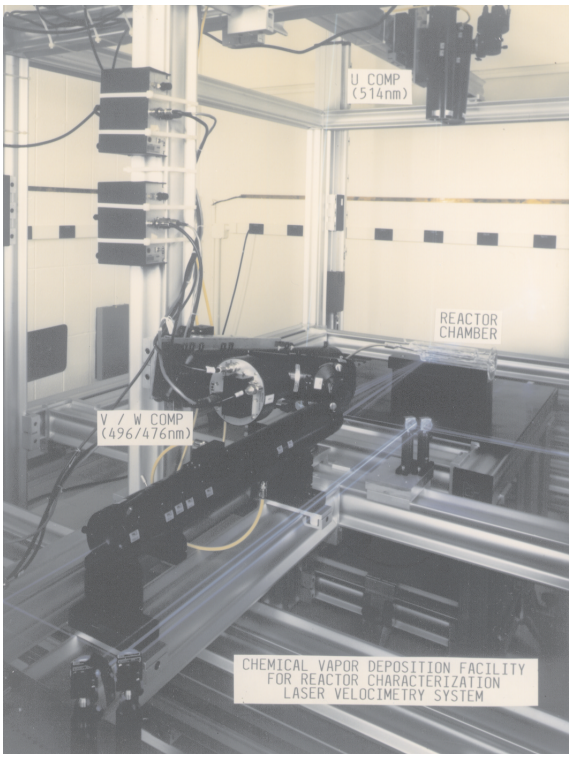

Figure 1.- The chemical vapor deposition facility with the orthogonal three component laser velocimeter.

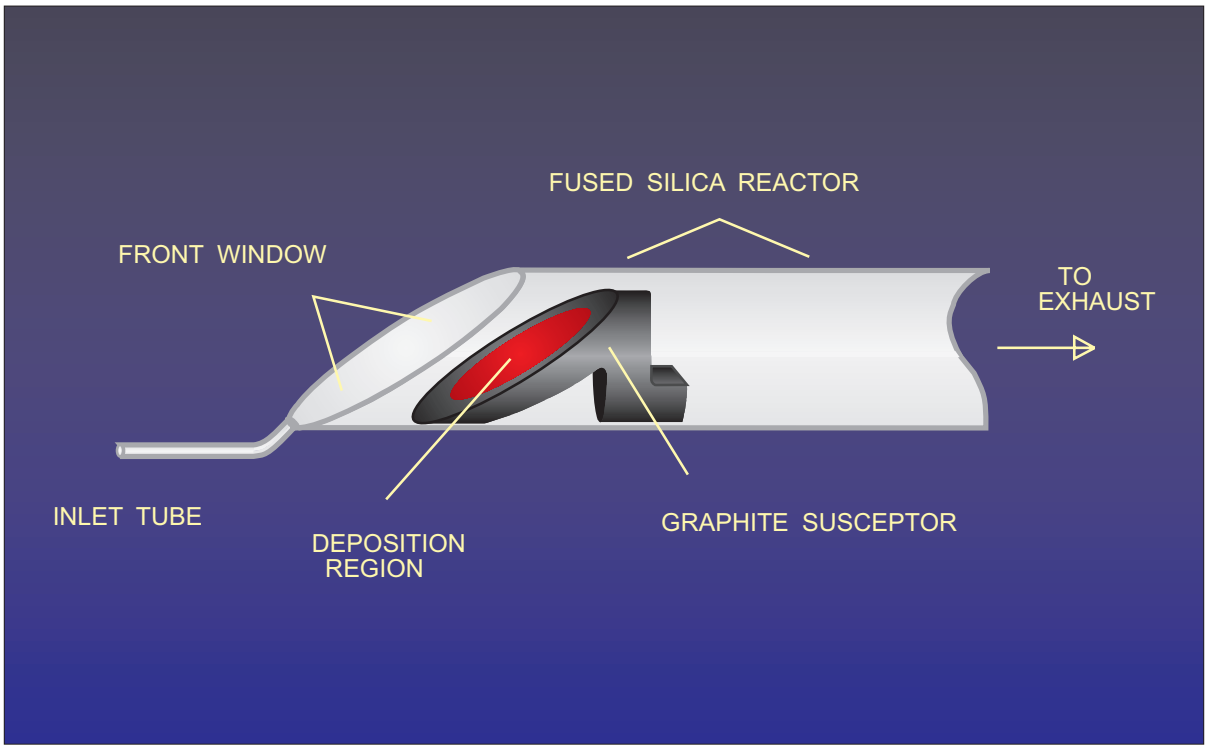

Figure 2.- Diagram of the metalorganic chemical vapor deposition reactor showing the tilted susceptor and front wall.

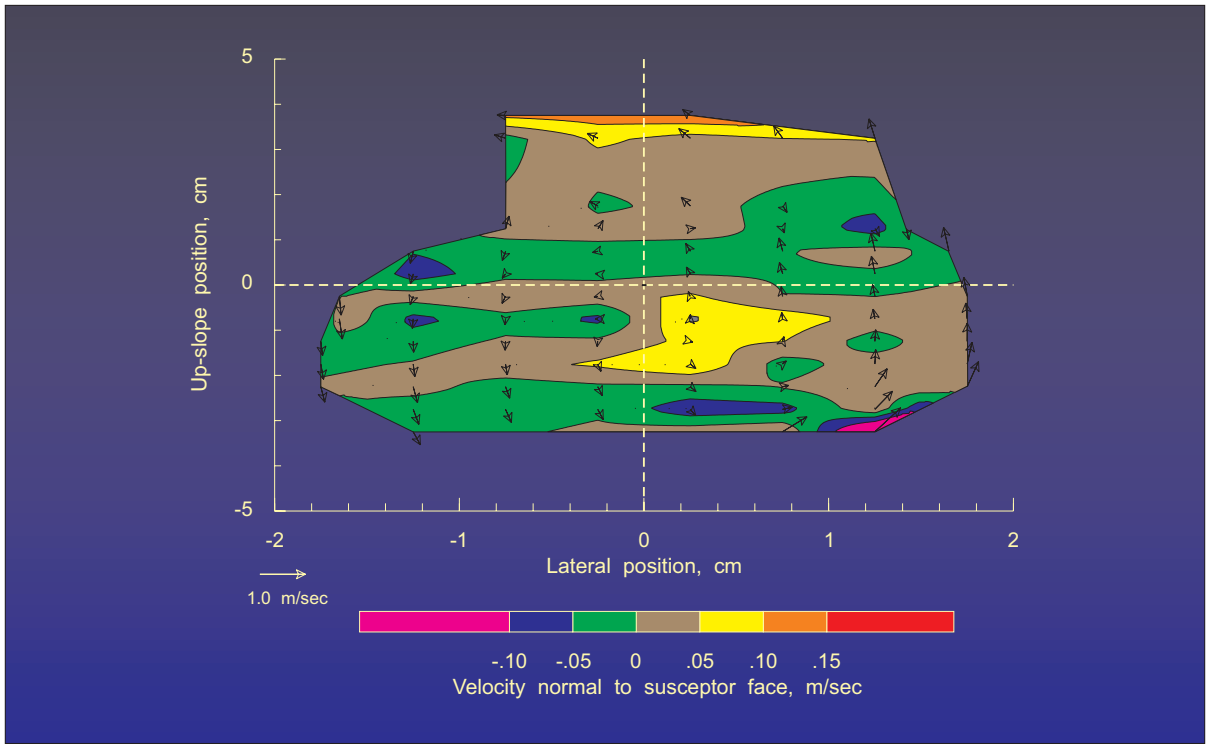

Figure 3.- Cold susceptor: Velocity components measured in a plane parallel to the face of the susceptor at a perpendicular distance of 6.2 mm.

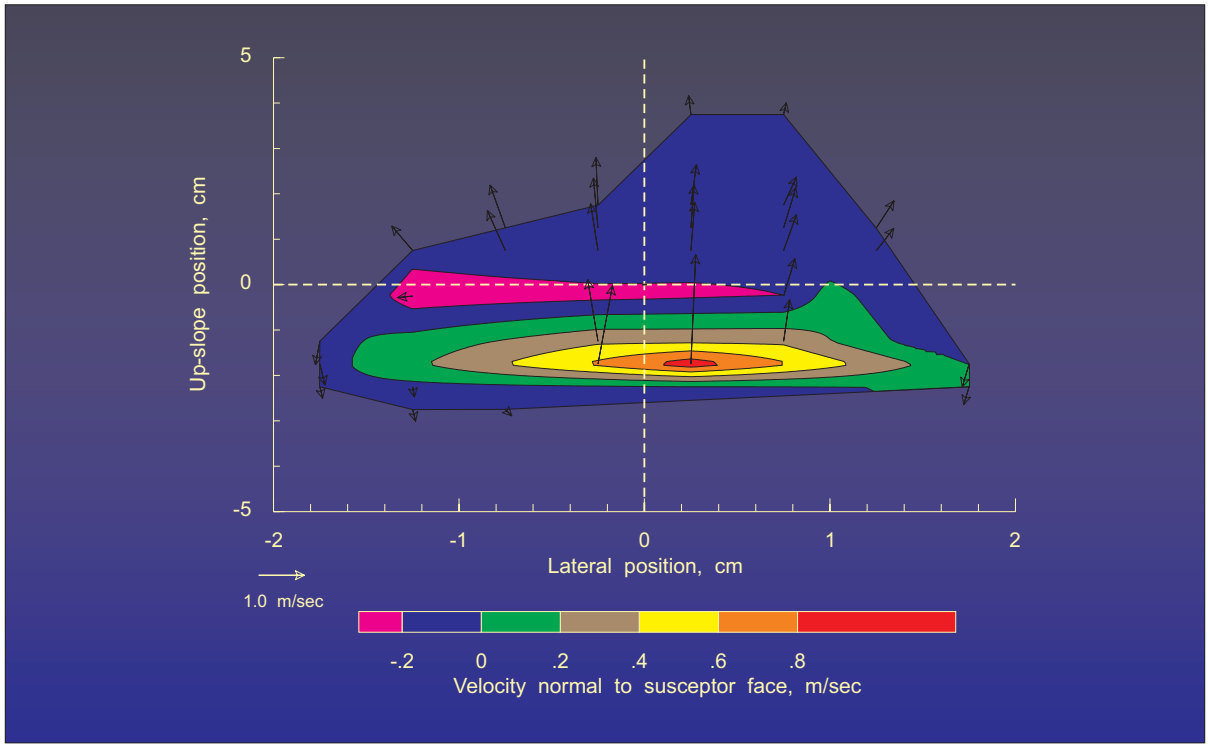

Figure 4.- Hot susceptor: Velocity components measured in a plane parallel to the face of the susceptor at a perpendicular distance of 6.2 mm.

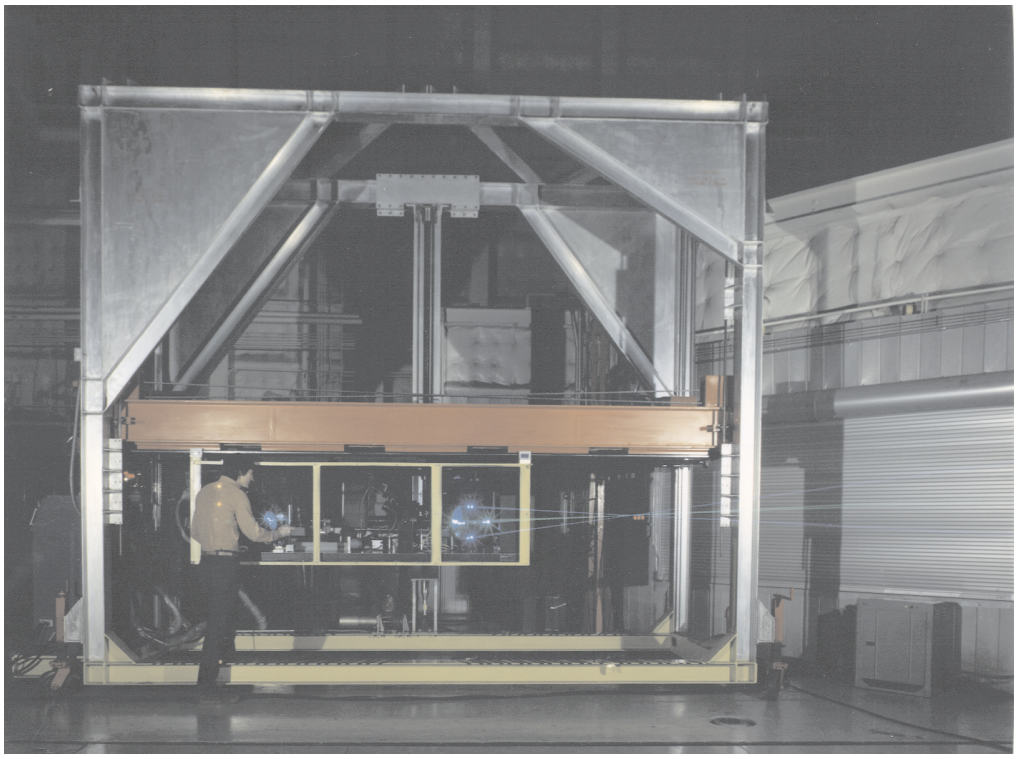

Figure 5.- The two component laser velocimeter in the 4x7-meter low speed wind tunnel.

Figure 6.- The two component laser velocimeter in the 4x7-meter low speed wind tunnel positioned for measurements above a helicopter rotor.

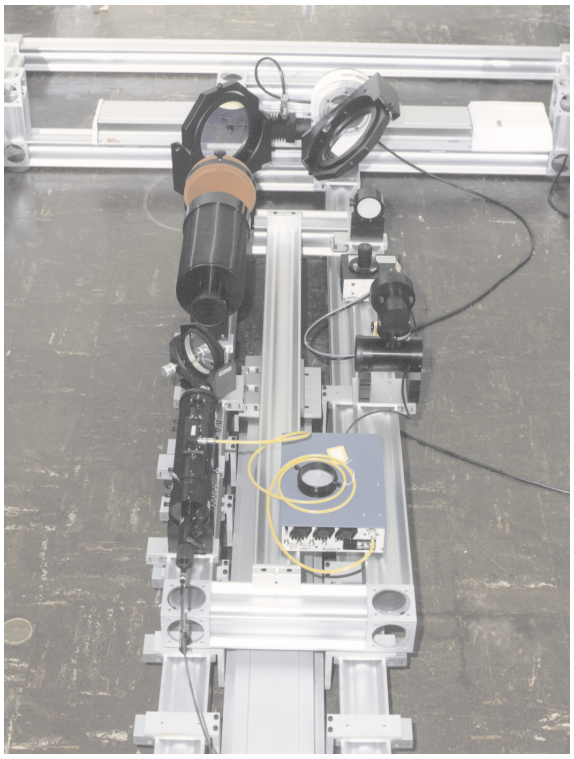

Figure 7.- The laser velocimeter to measure the cross tunnel velocity component in the 4x7-meter low speed wind tunnel.

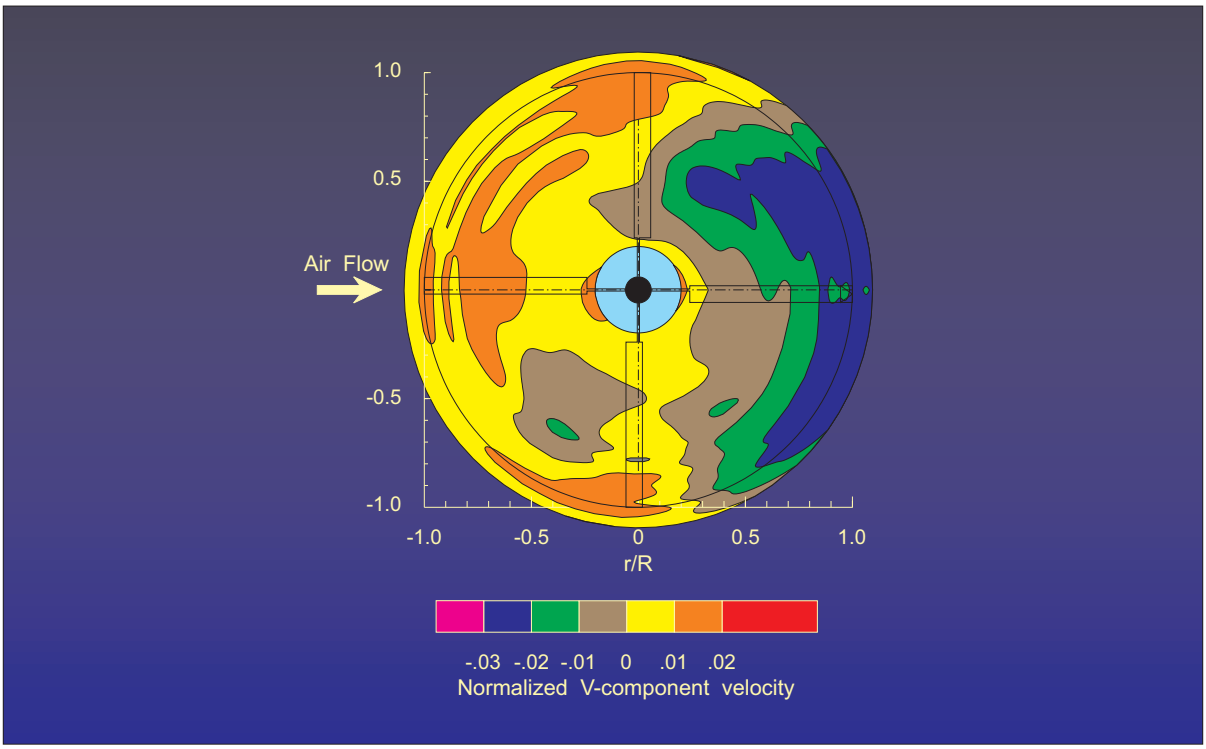

Figure 8.- Freestream removed V-component of velocity 1.0 chord above the helicopter rotor disk at azimuth angle = 0.0^{0}.

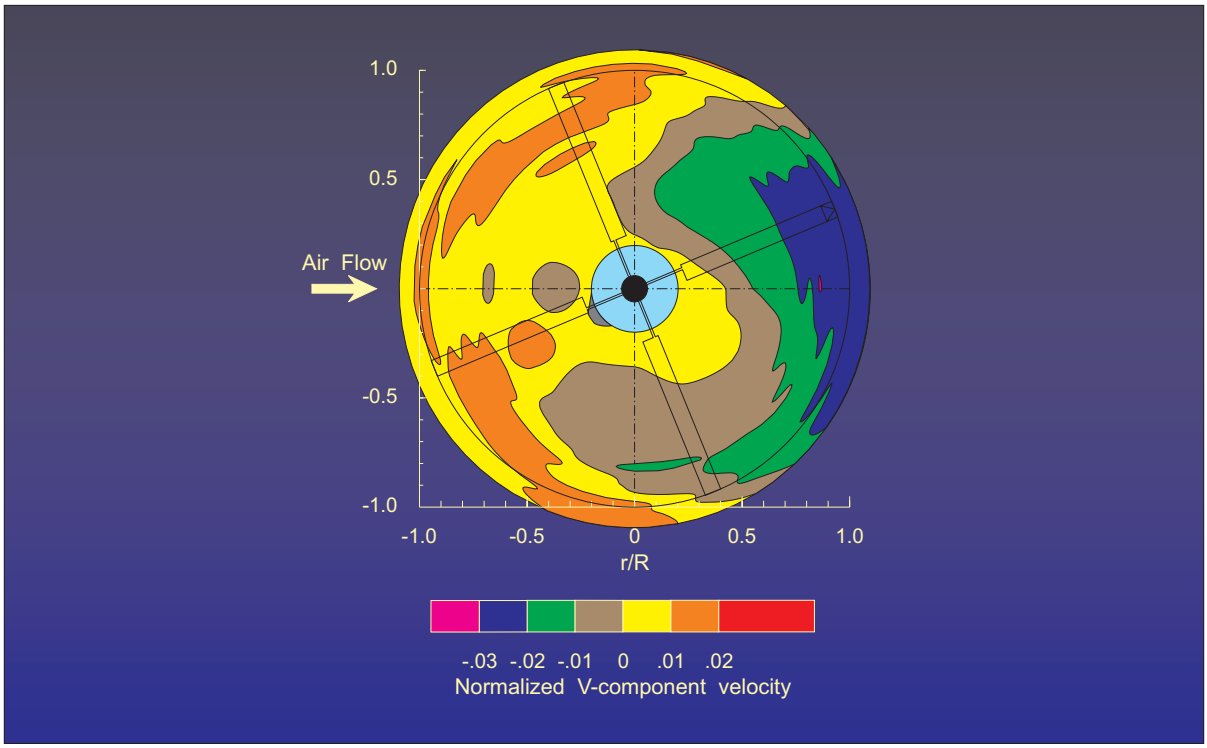

Figure 9.- Freestream removed V-component of velocity 1.0 chord above the helicopter rotor disk at azimuth angle = 22.5°.

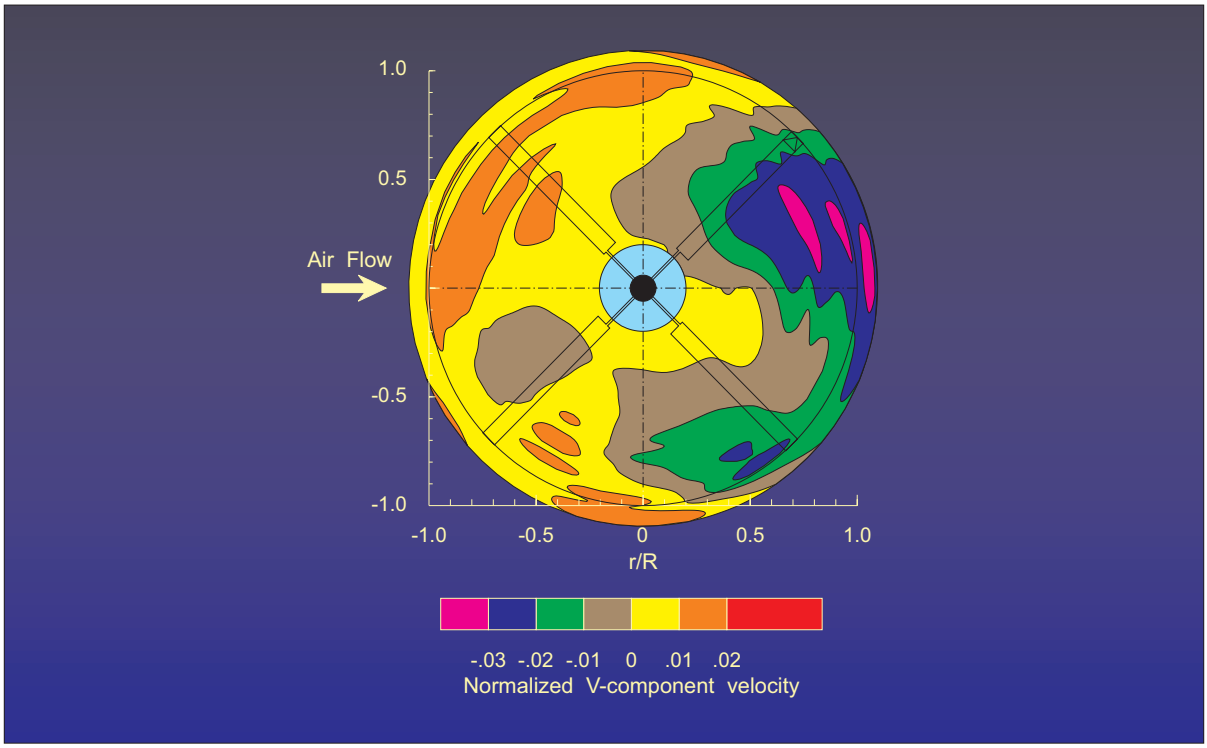

Figure 10.- Freestream removed V-component of velocity 1.0 chord above the helicopter rotor disk at azimuth angle = 45.0°.

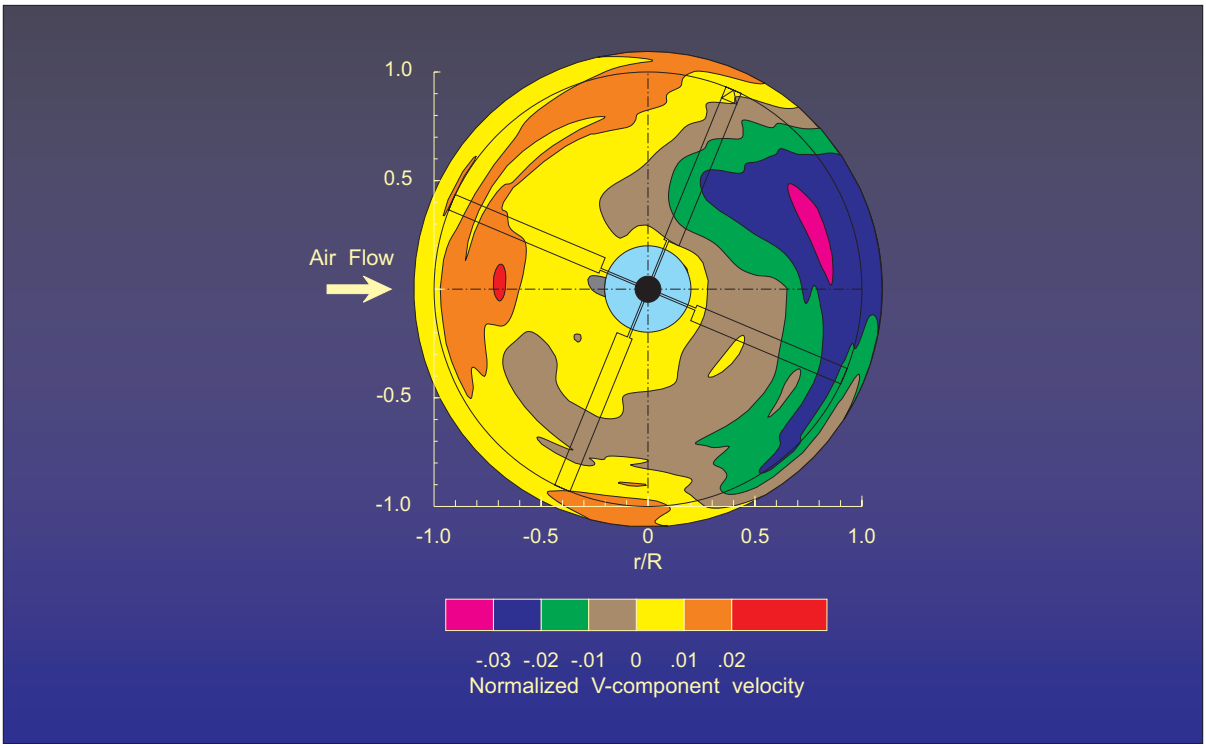

Figure 11.- Freestream removed V-component of velocity 1.0 chord above the helicopter rotor disk at azimuth angle = 67.5^{o}.

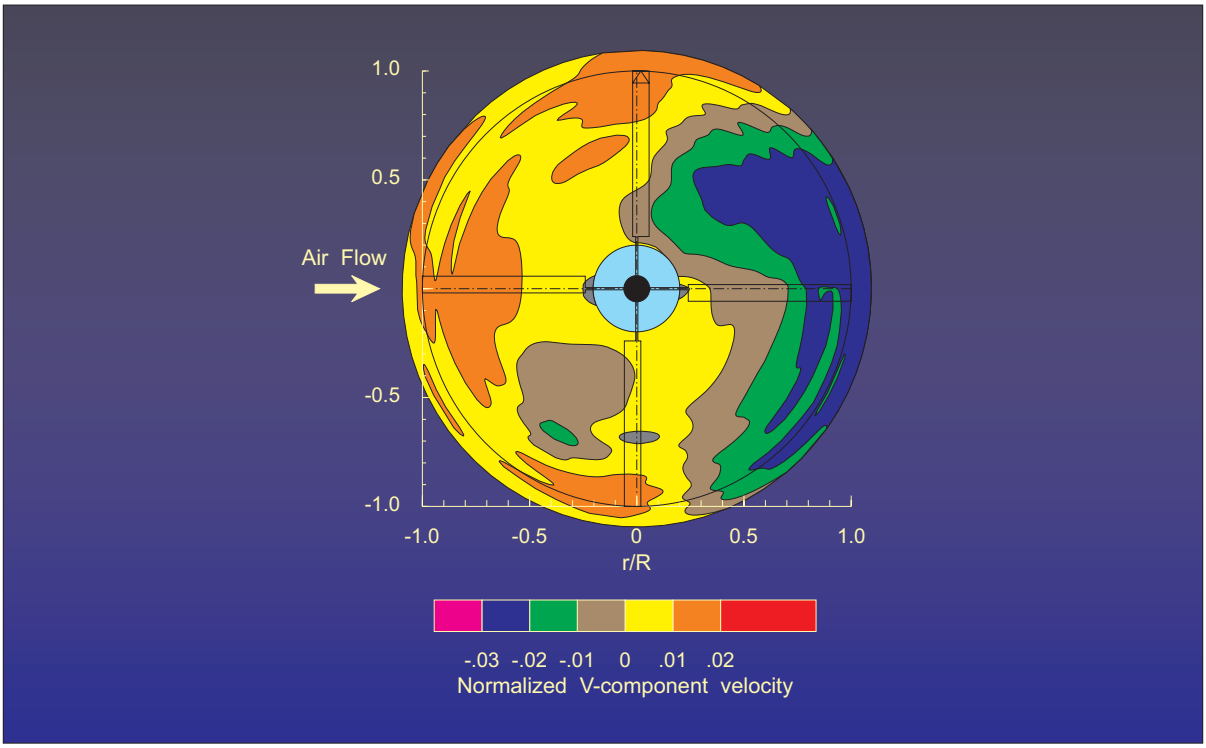

Figure 12.- Freestream removed V-component of velocity 1.0 chord above the helicopter rotor disk at azimuth angle = 90.0^{o}.

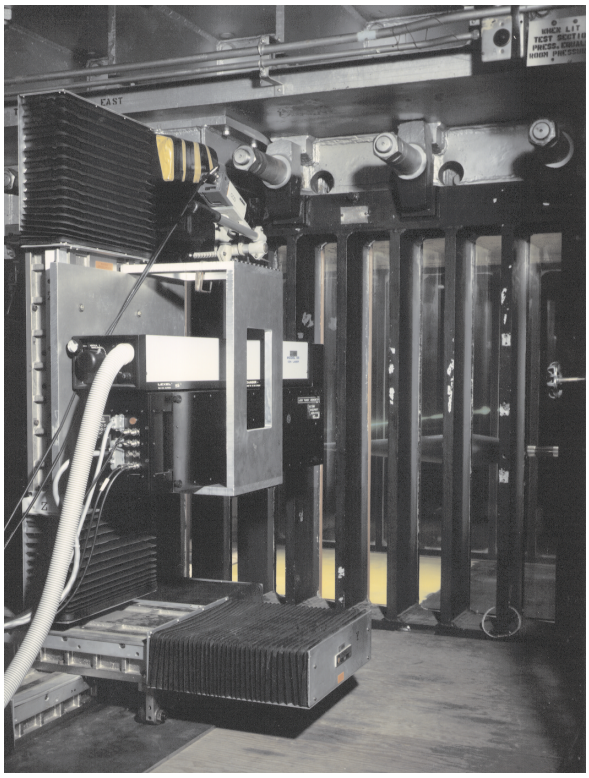

Figure 13.- Laser transit anemometer mounted next to the Unitary Plan Wind Tunnel.

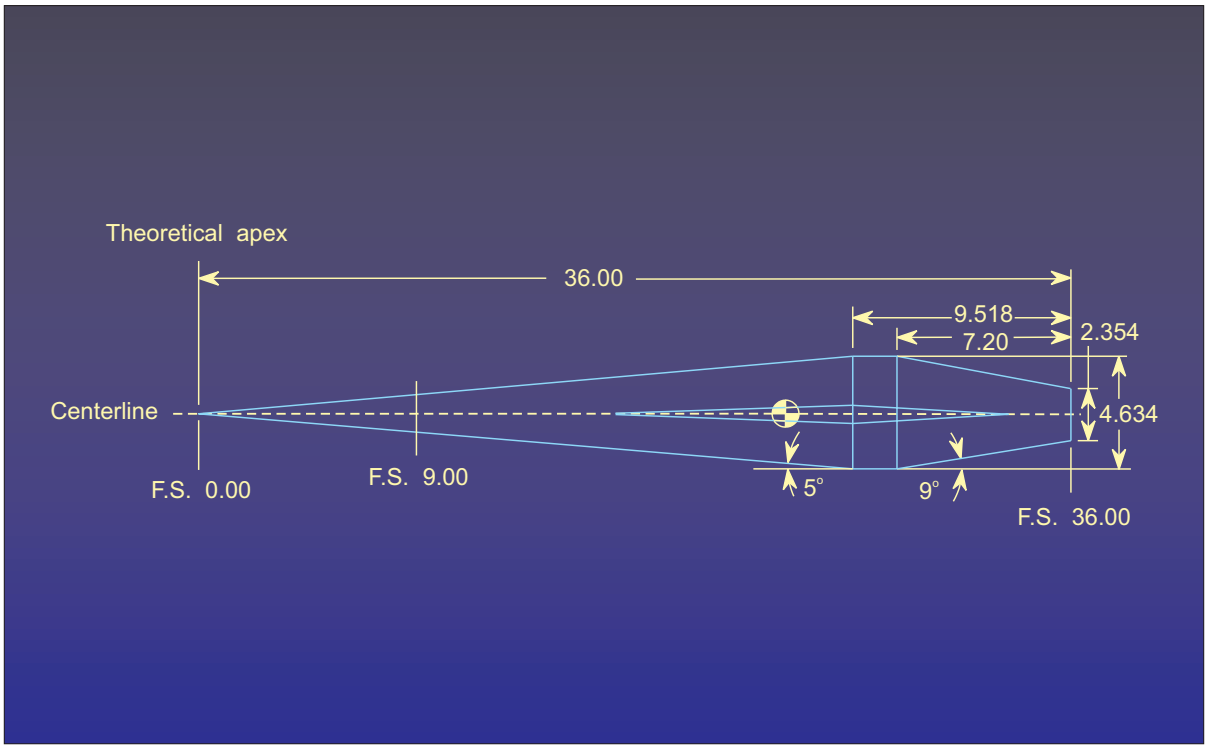

Figure 14.- Diagram of the slender cone model.

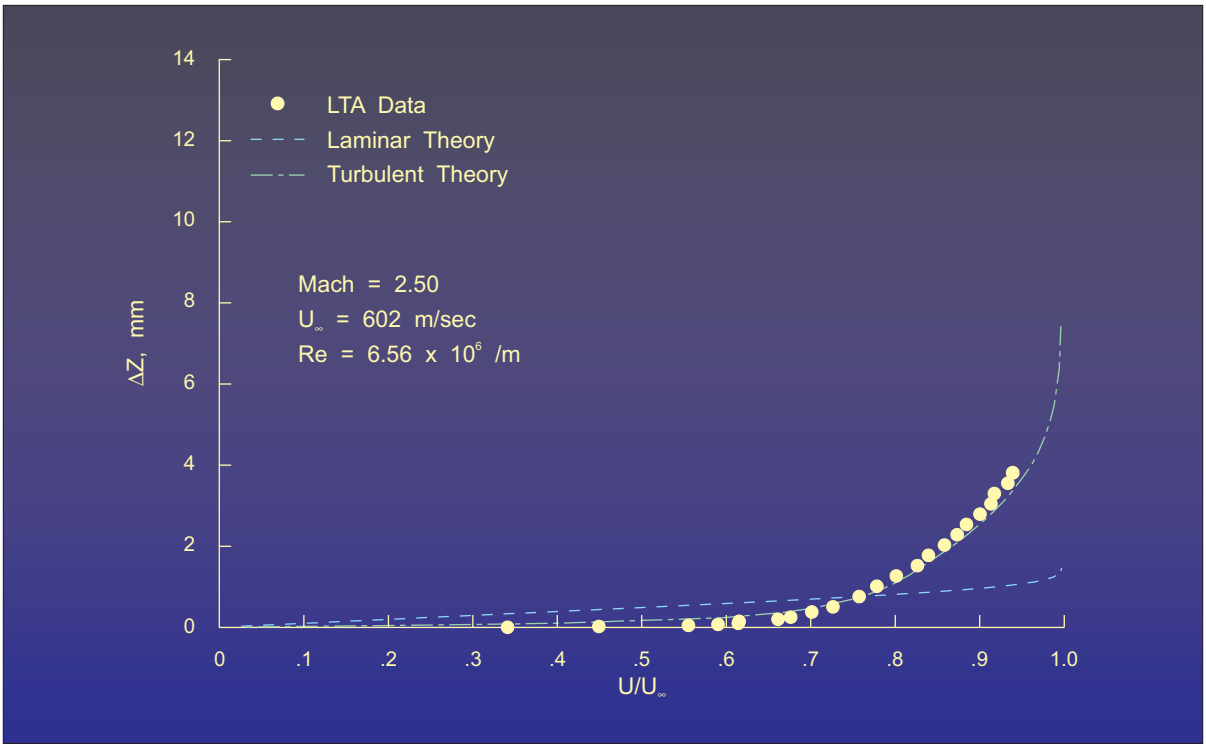

Figure 15.- Normalized mean velocity profiles in the boundary layer above the slender cone model at Mach 2.5.

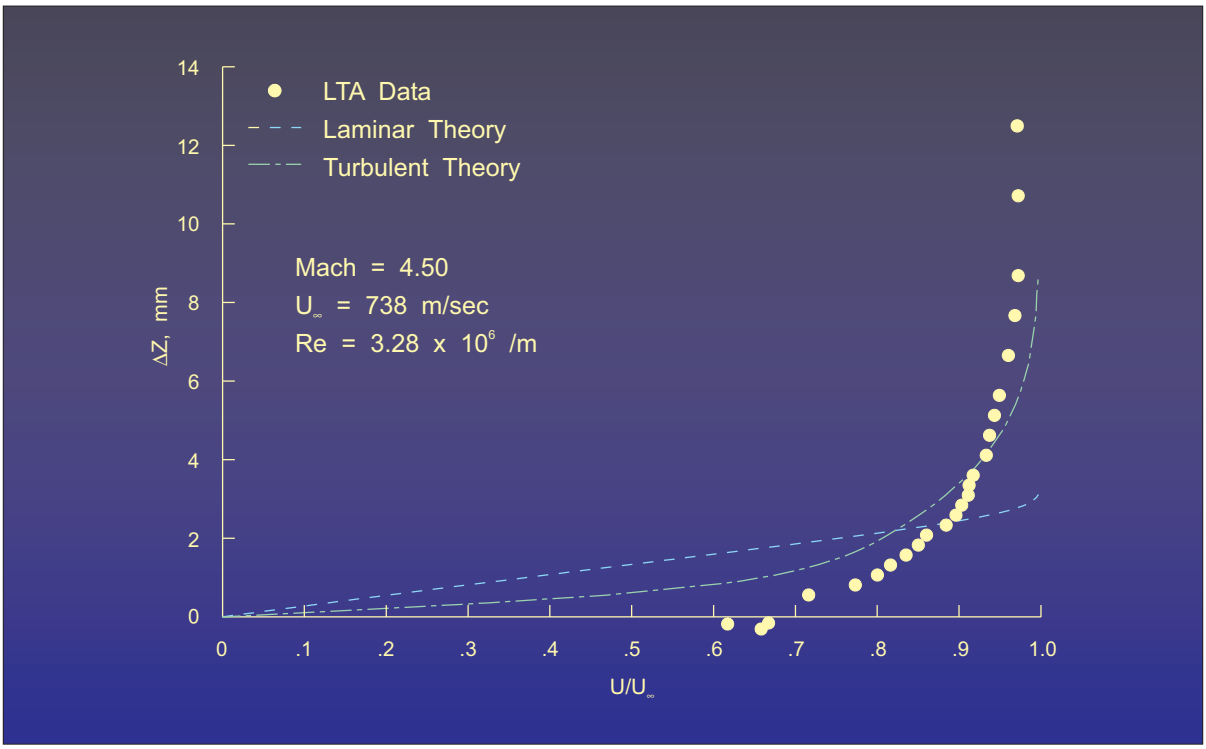

Figure 16.- Normalized mean velocity profiles in the boundary layer above the slender cone model at Mach 4.5.

Figure 17.- Basic Aerodynamic Research Tunnel (BART) with the orthogonal three component laser velocimeter.

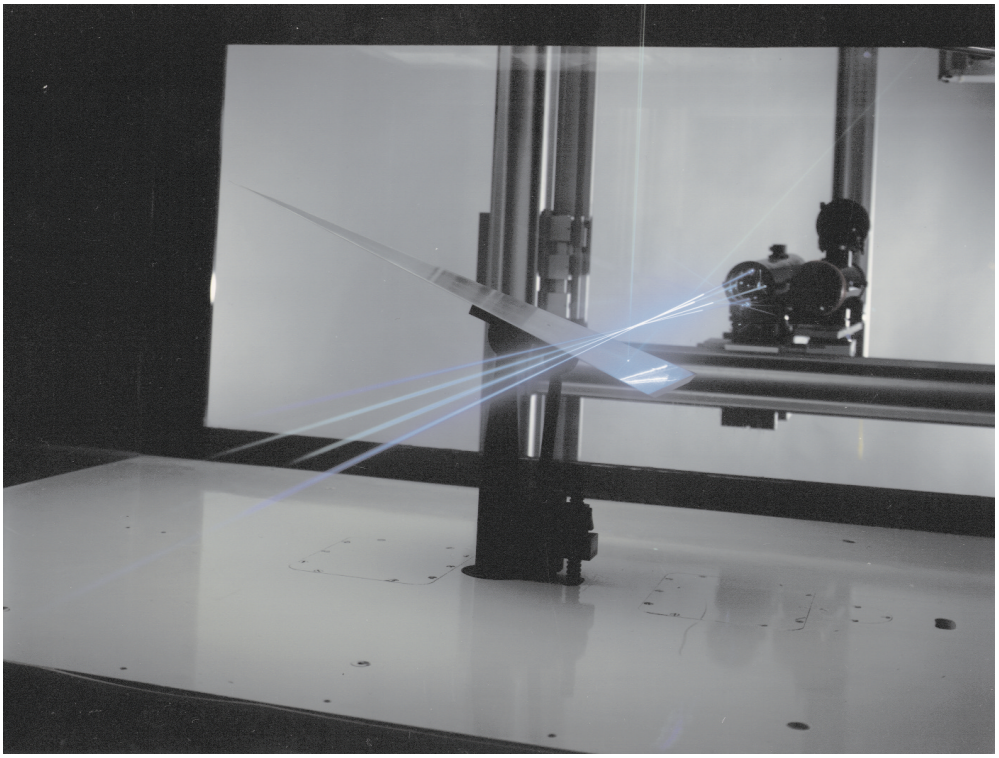

Figure 18.- View of the 75^{o} delta wing in BART with the crossing laser beams from the orthogonal three component laser velocimeter.

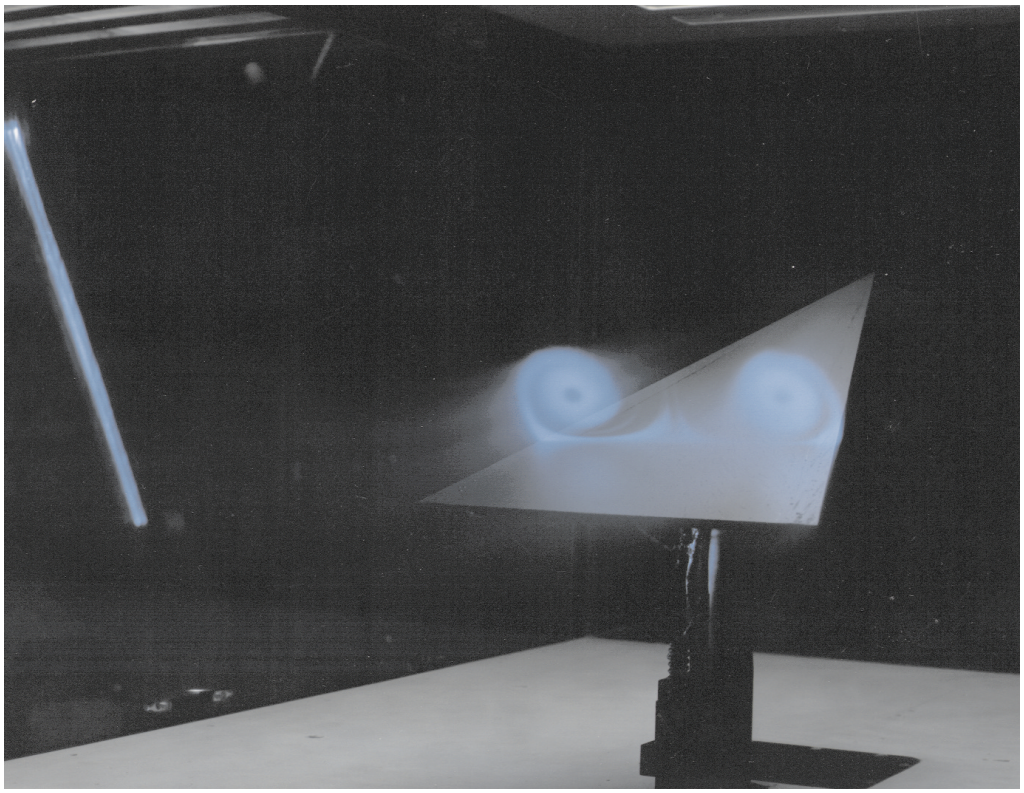

Figure 19.- Laser light sheet flow visualization of the vortex flow above the 75^{o} delta wing at an angle-of-attack = 20.5^{o}.

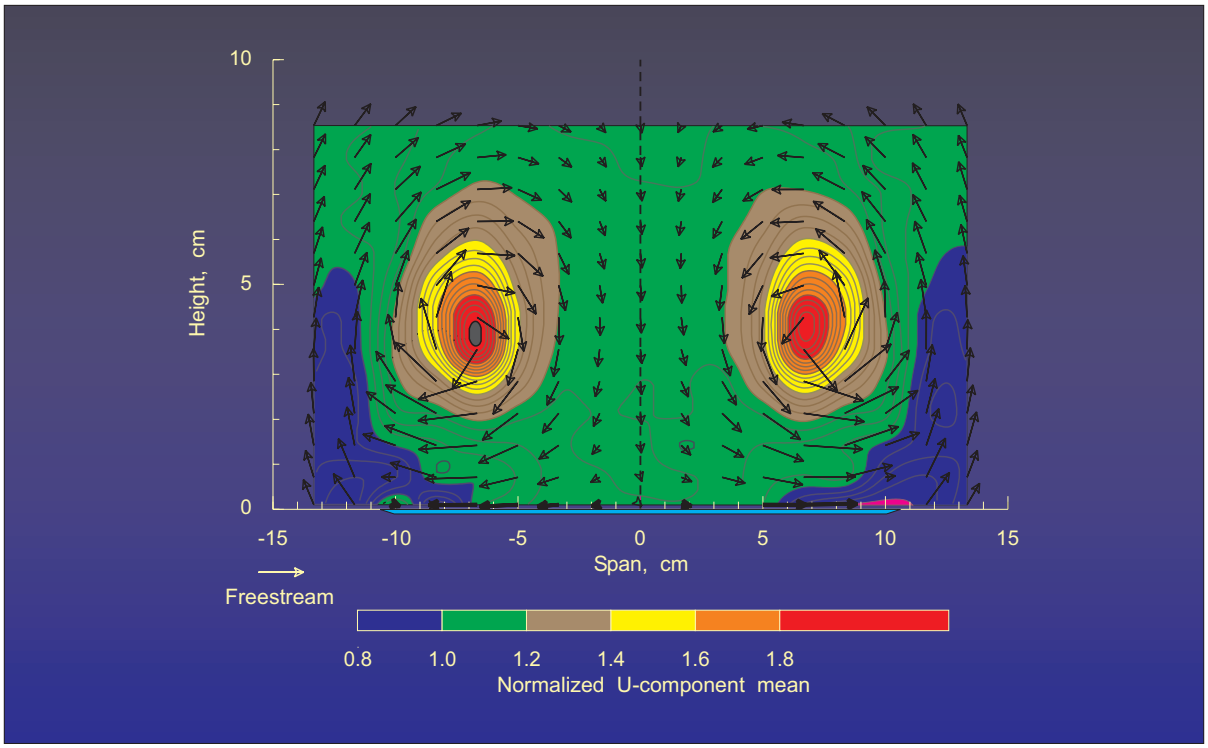

Figure 20.- Mean velocity measurements of the vortex flow above the 75° delta wing at an angle-of-attack = 20.5°.

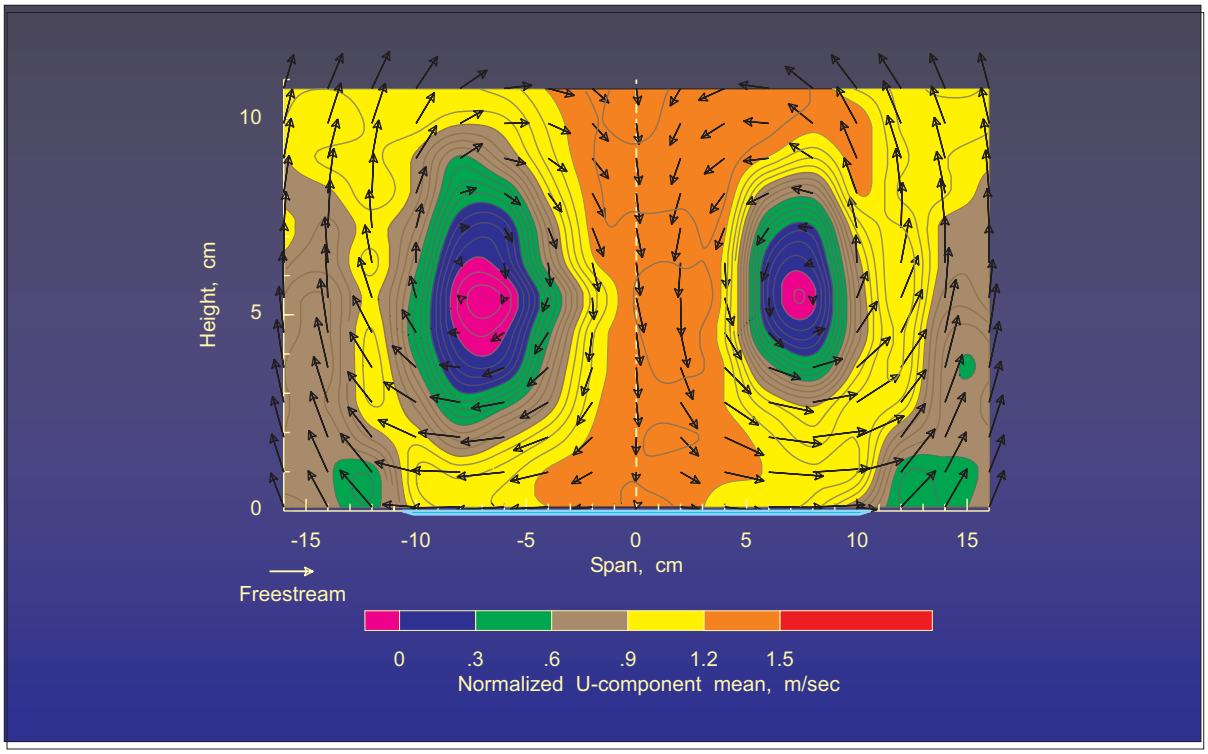

Figure 21.- Mean velocity measurements of the vortex flow above the 75° delta wing at an angle-of-attack = 40.0°.

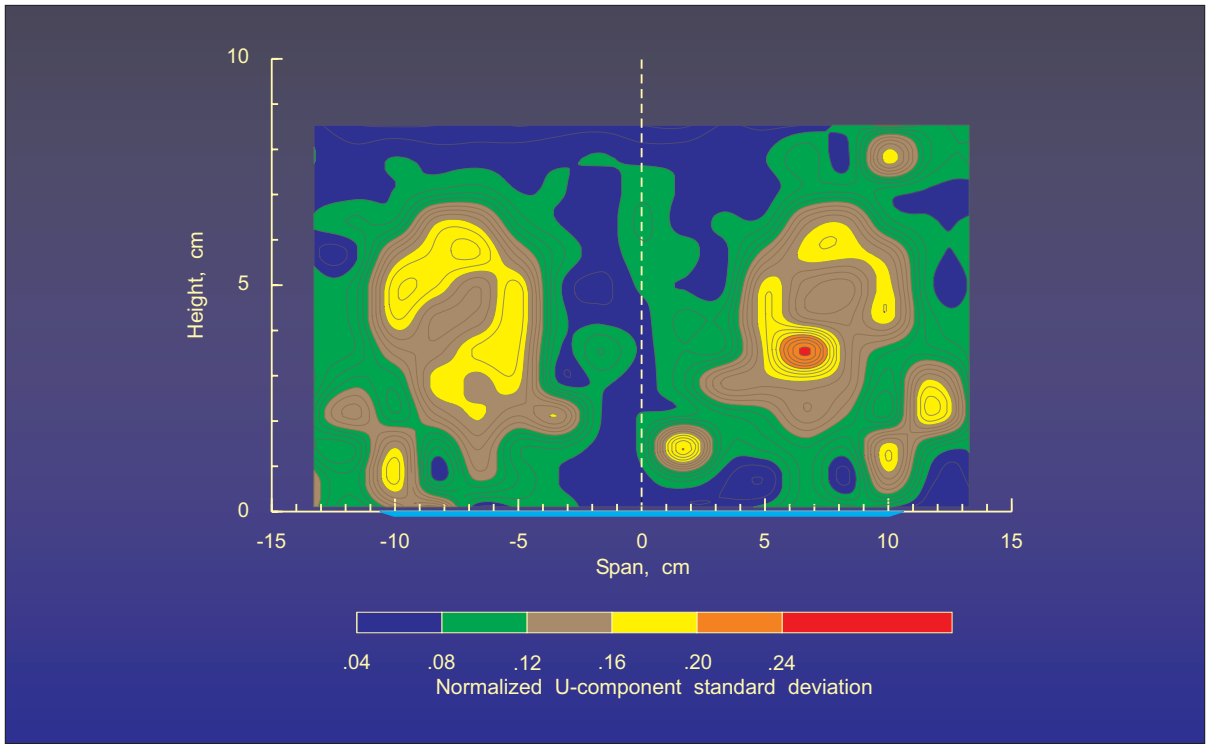

Figure 22.- Contours of streamwise normalized standard deviation of the vortex flow above the 75° delta wing at an angle-of-attack = 20.5°.

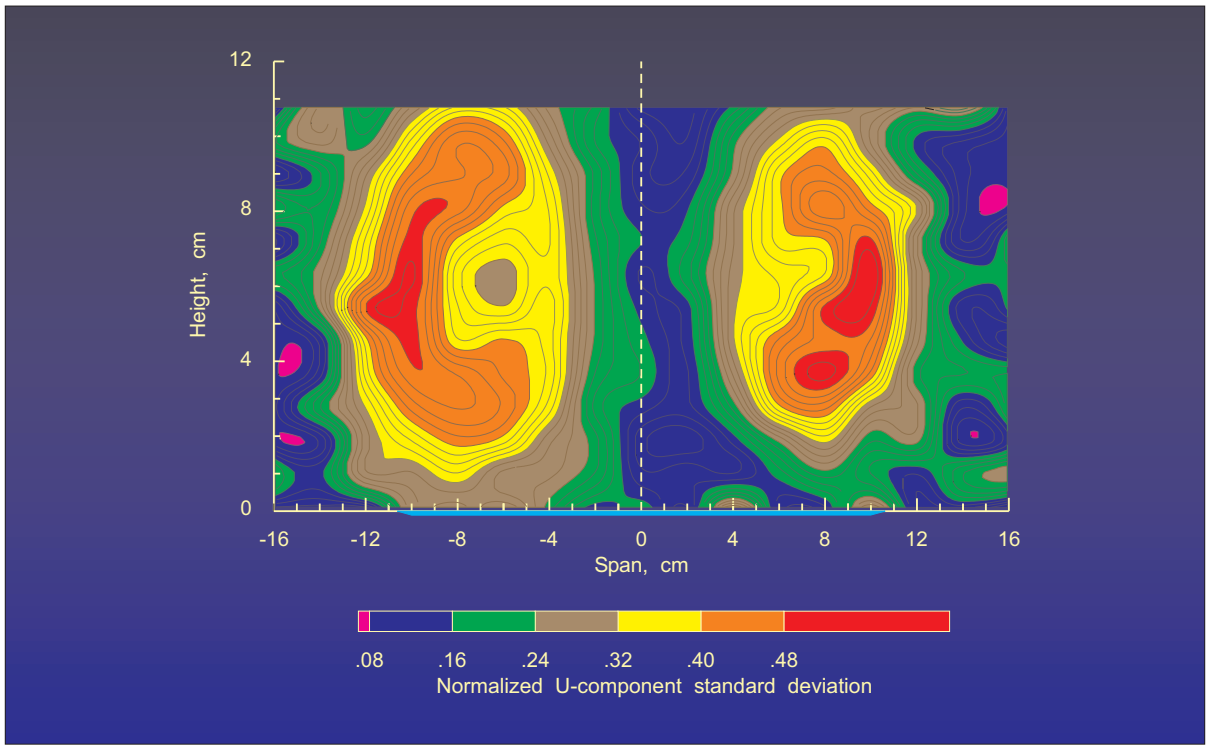

Figure 23.- Contours of streamwise normalized standard deviation of the vortex flow above the 75° delta wing at an angle-of-attack = 40.0°.

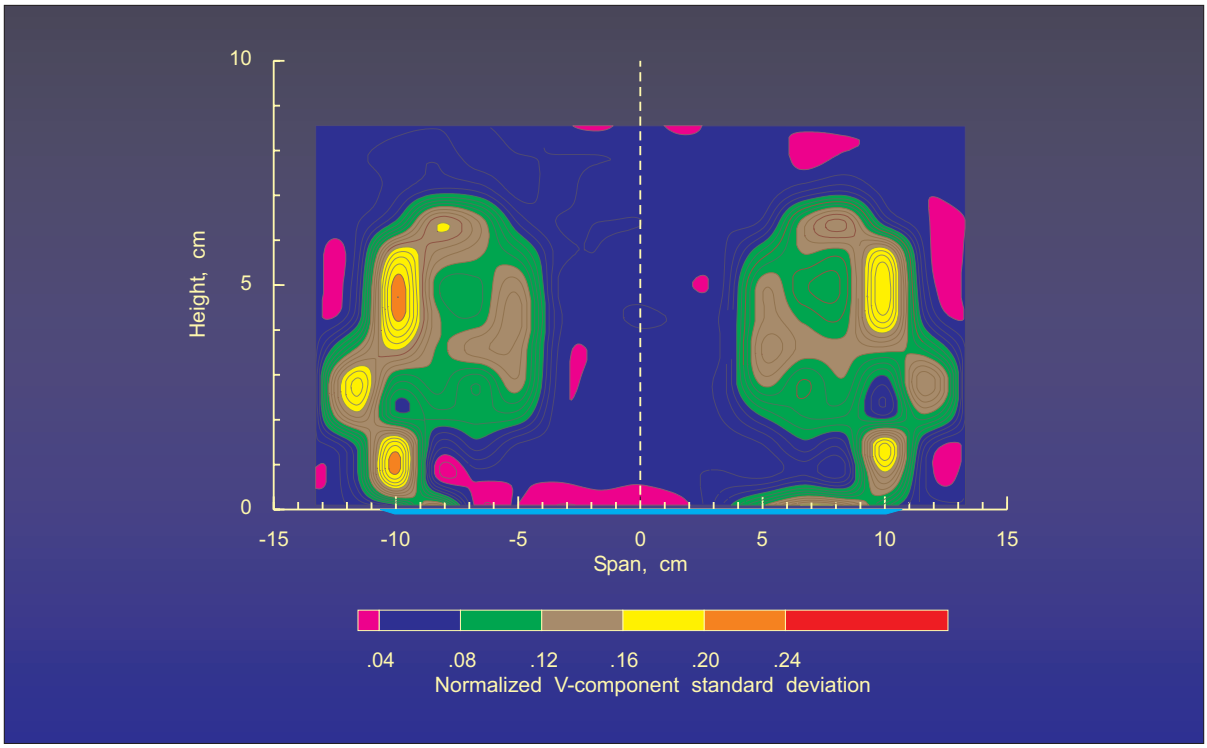

Figure 24.- Contours of vertical normalized standard deviation of the vortex flow above the 75° delta wing at an angle-of-attack = 20.5°.

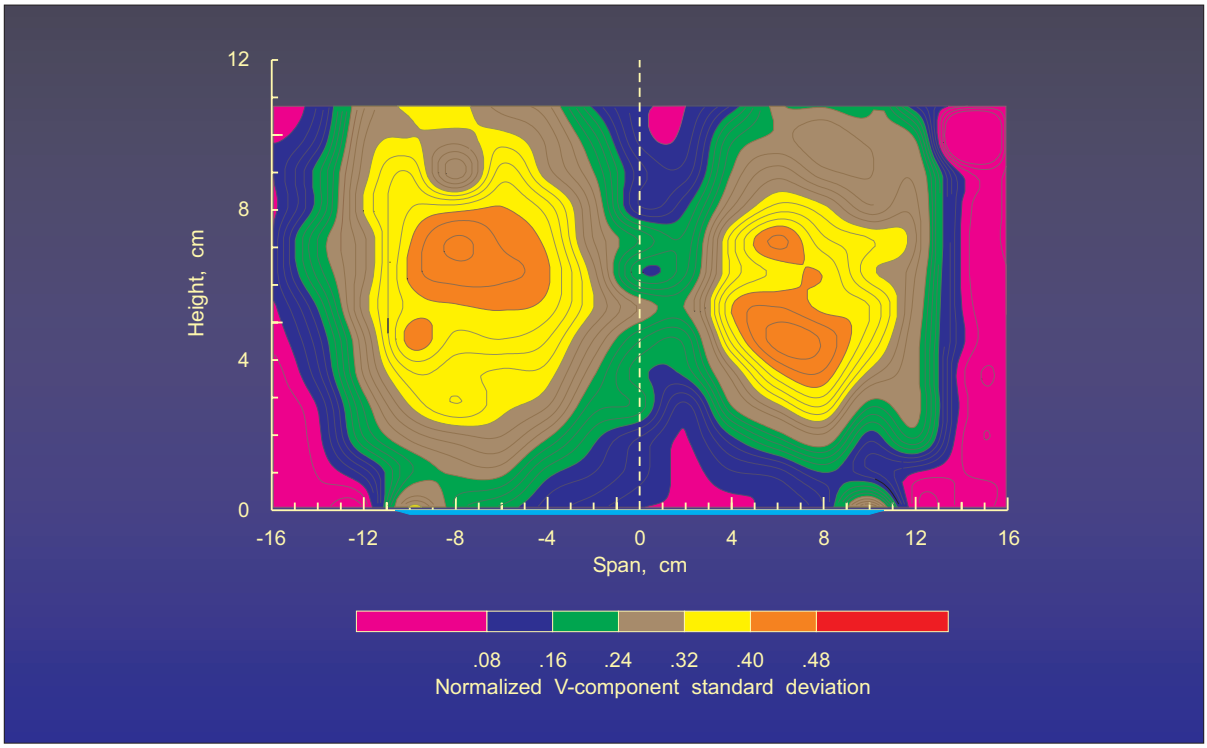

Figure 25.- Contours of vertical normalized standard deviation of the vortex flow above the 75° delta wing at an angle-of-attack = 40.0°.

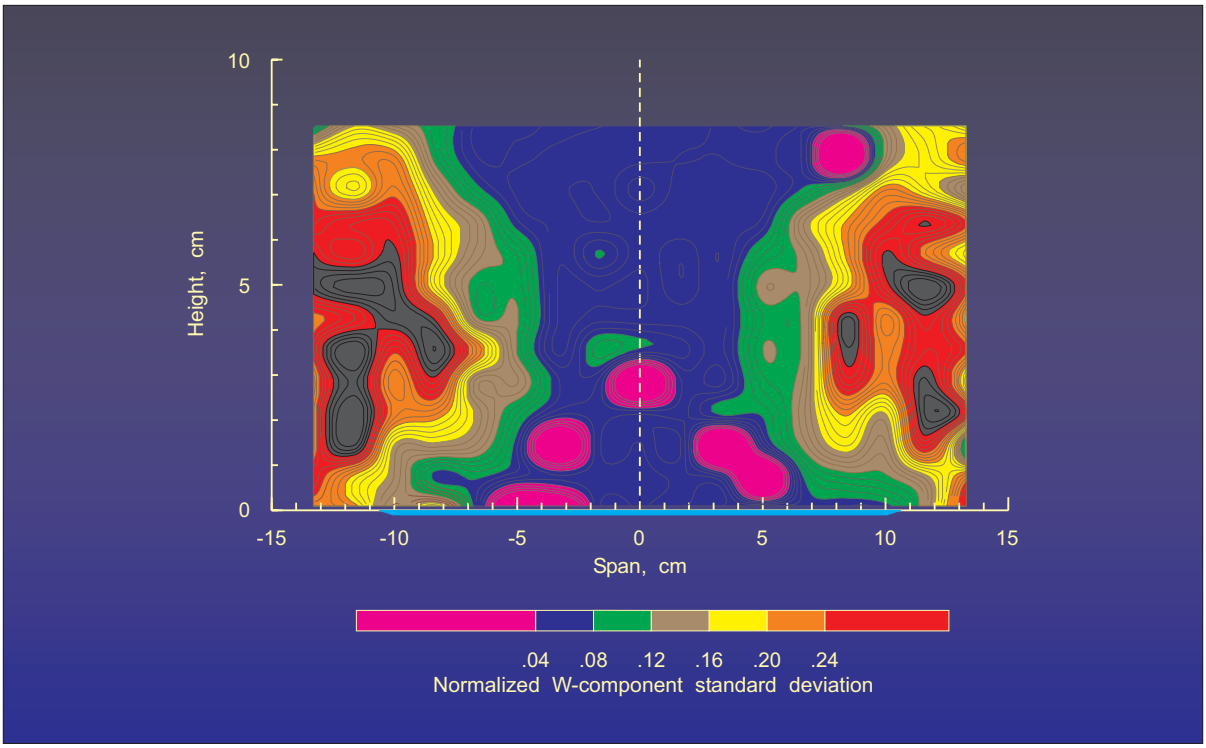

Figure 26.- Contours of traverse normalized standard deviation of the vortex flow above the 75° delta wing at an angle-of-attack = 20.5°.

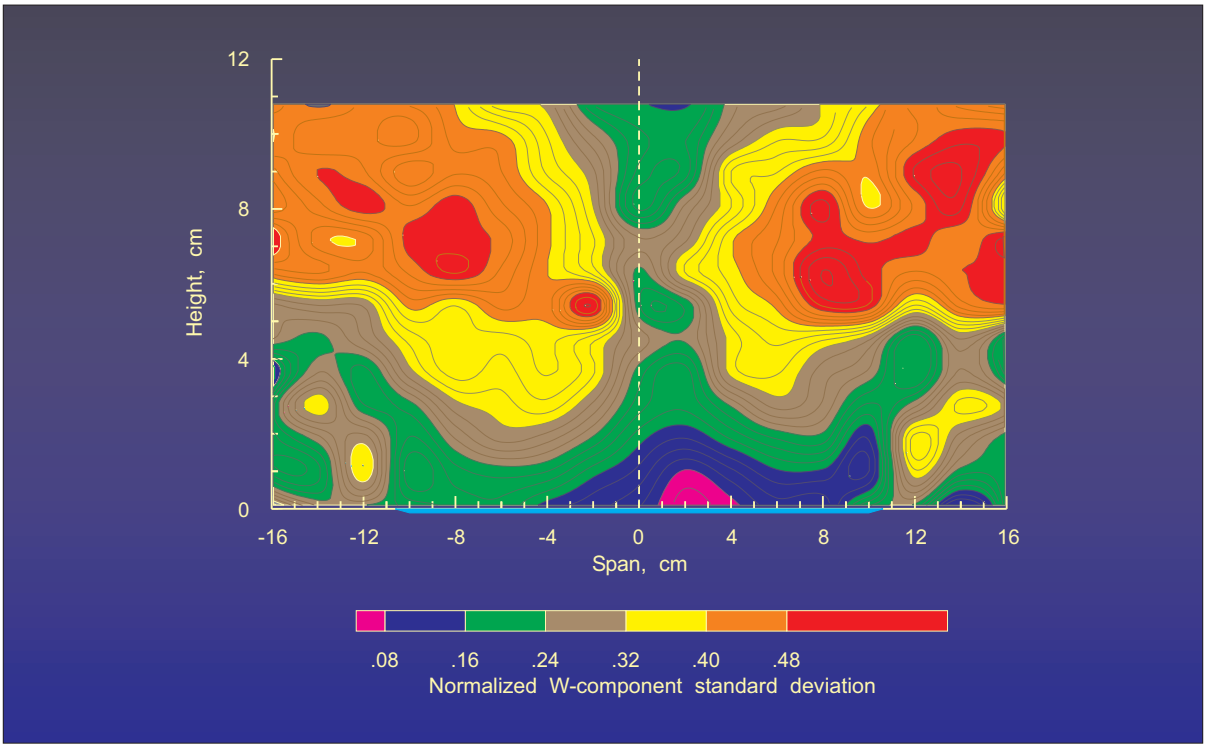

Figure 27.- Contours of traverse normalized standard deviation of the vortex flow above the 75° delta wing at an angle-of-attack = 40.0°.

Figure 28.- Photograph of an F-18 fighter at high angle of attack.

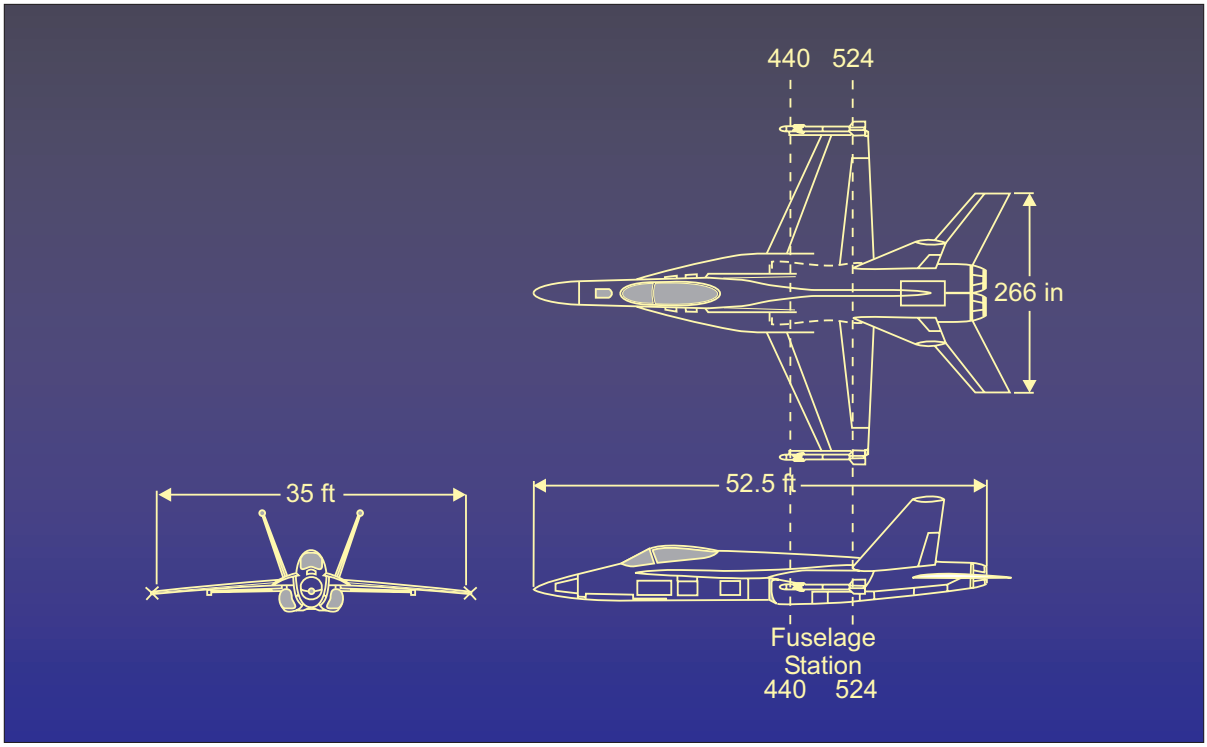

Figure 29.- Three-view diagram of the YF-17 configuration.

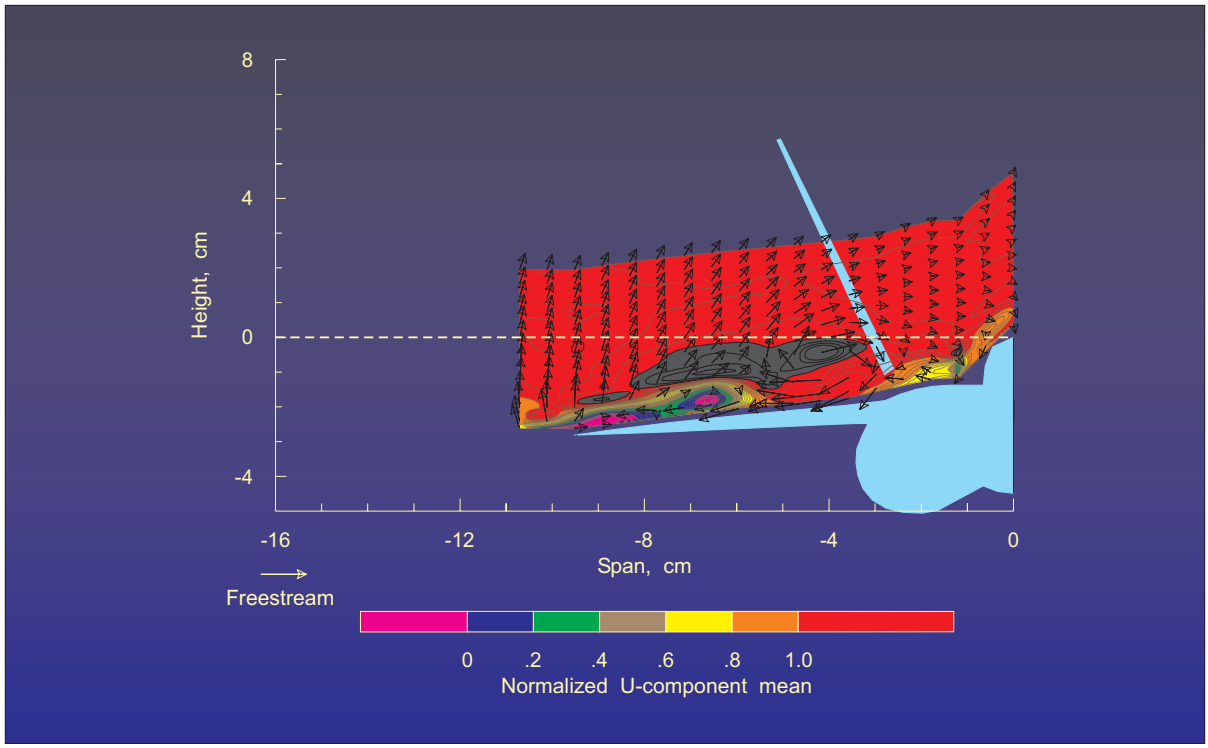

Figure 30.- Mean velocity measurements of the vortex flow above the YF-17 model at an angle-of-attack = 15.0°, station 440.

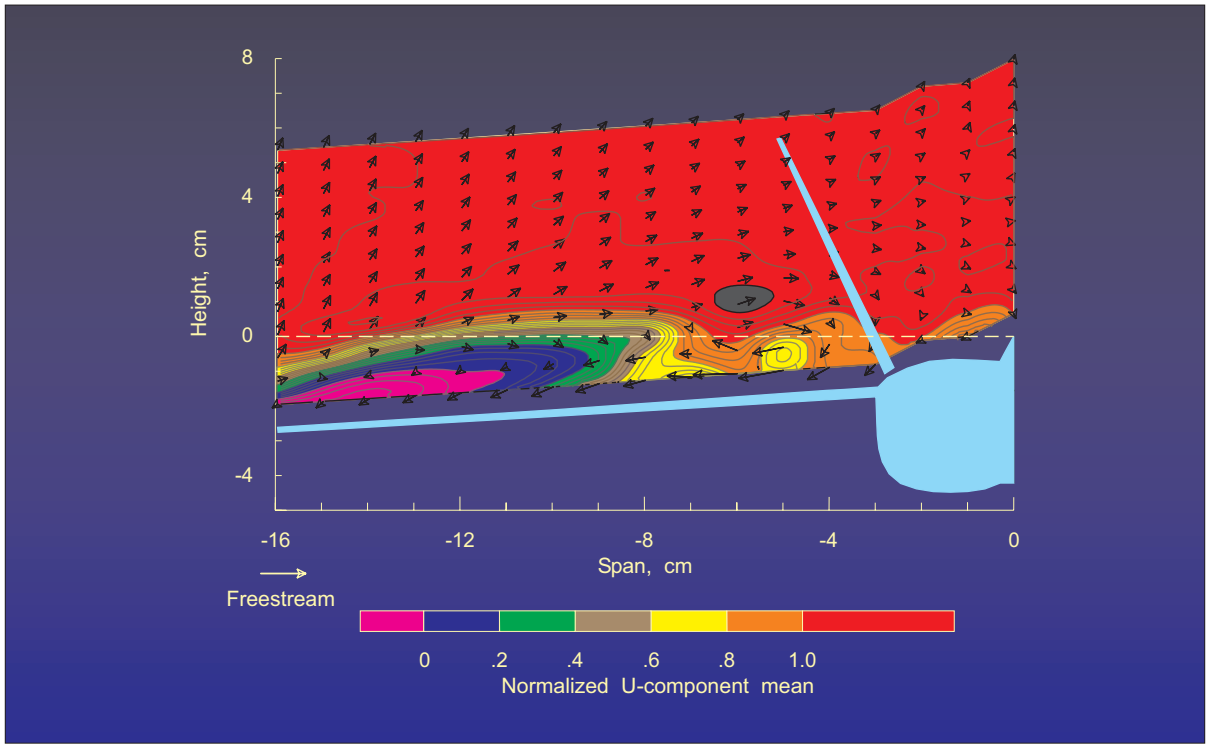

Figure 31.- Mean velocity measurements of the vortex flow above the YF-17 model at an angle-of-attack = 15.0°, station 524.

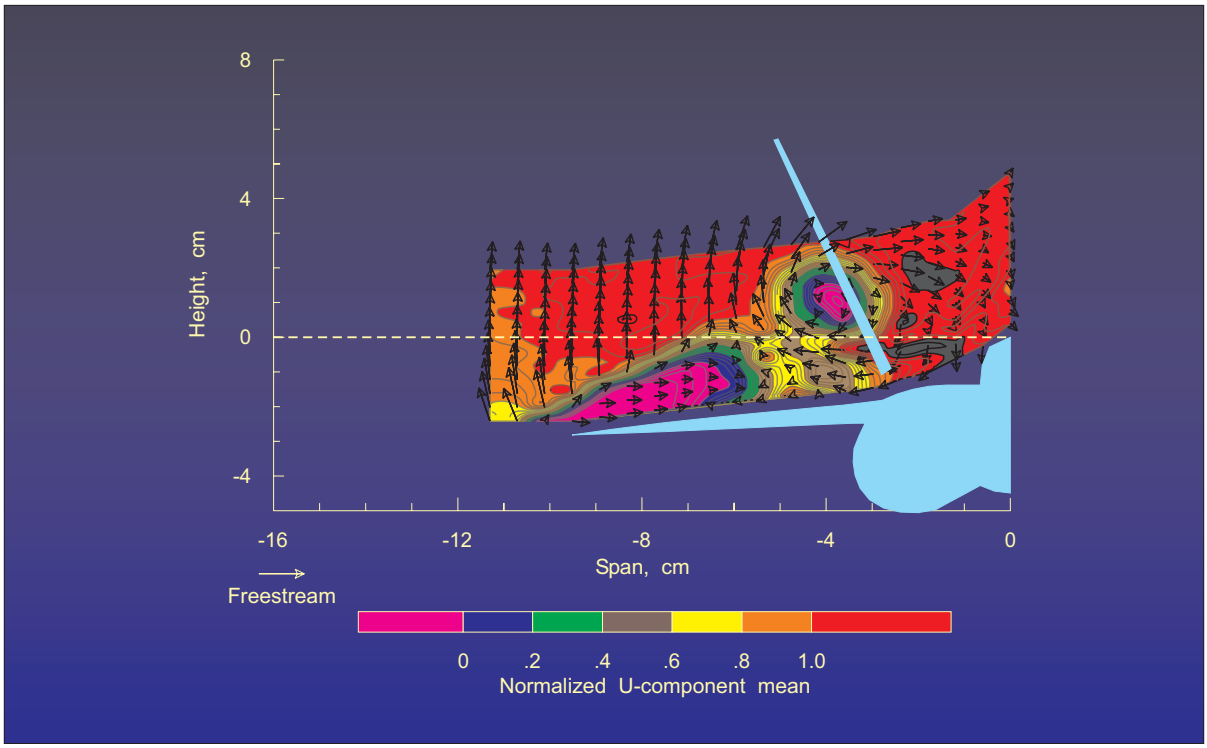

Figure 32.- Mean velocity measurements of the vortex flow above the YF-17 model at an angle-of-attack = 25.0^{0}, station 440.

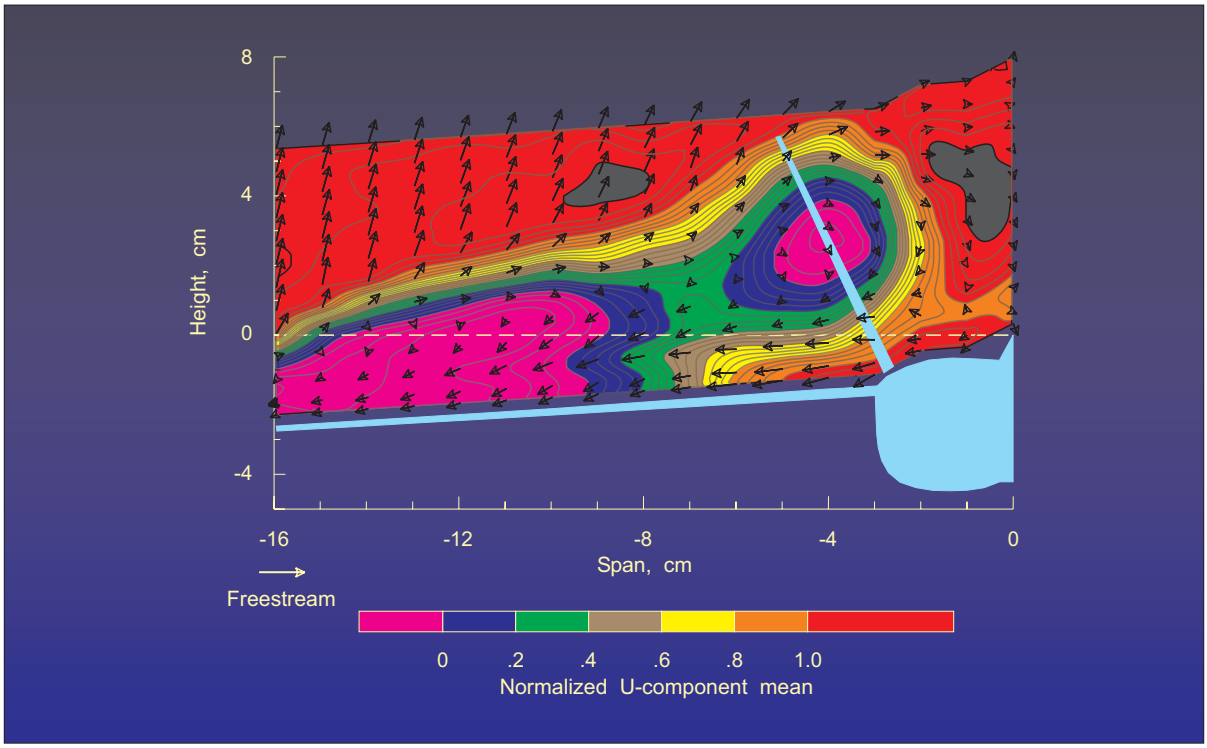

Figure 33.- Mean velocity measurements of the vortex flow above the YF-17 model at an angle-of-attack = 25.0^{0}, station 524.

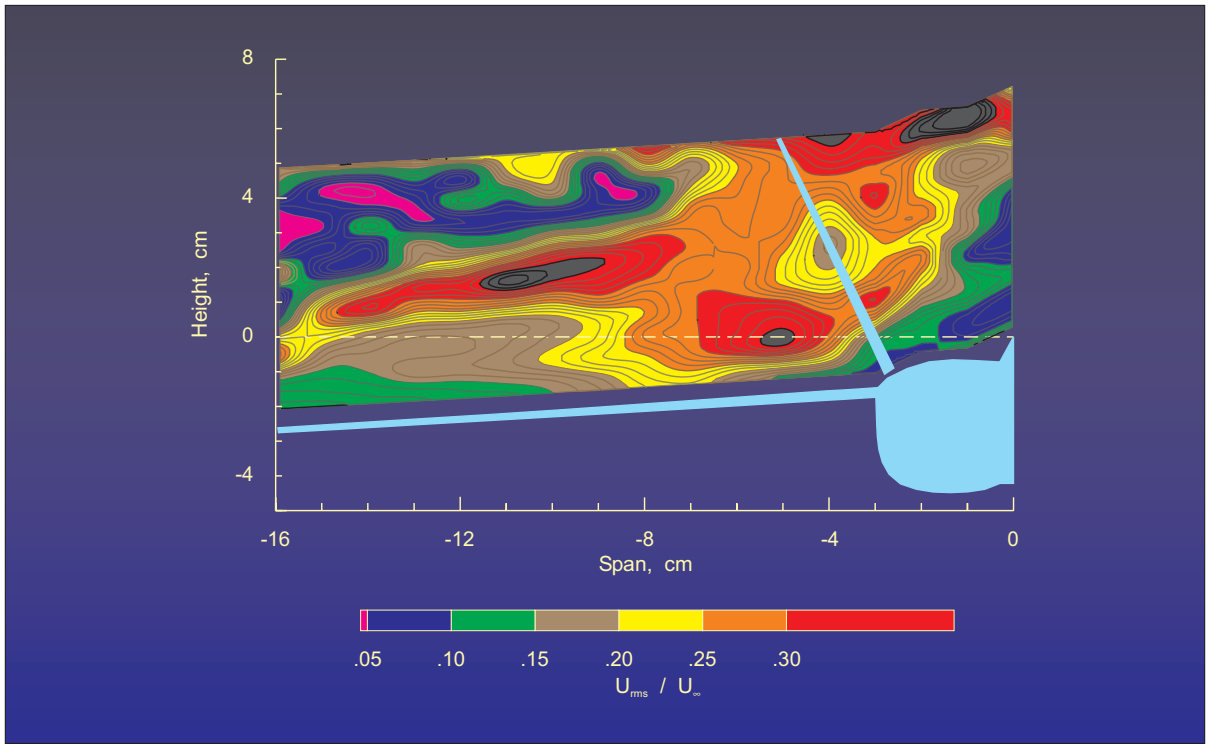

Figure 34.- Contours of streamwise normalized standard deviation of the vortex flow above the YF-17 model at an angle-of-attack = 25.0°, station 524.

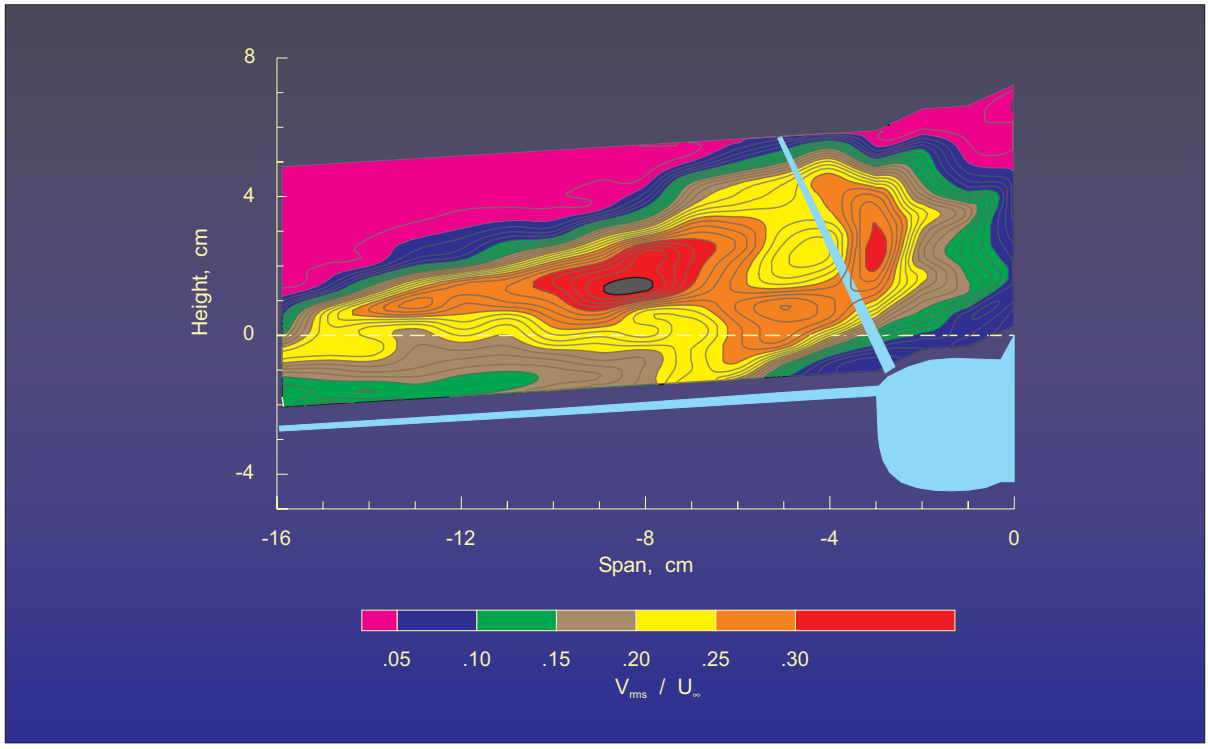

Figure 35.- Contours of vertical normalized standard deviation of the vortex flow above the YF-17 model at an angle-of-attack = 25.0°, station 524.

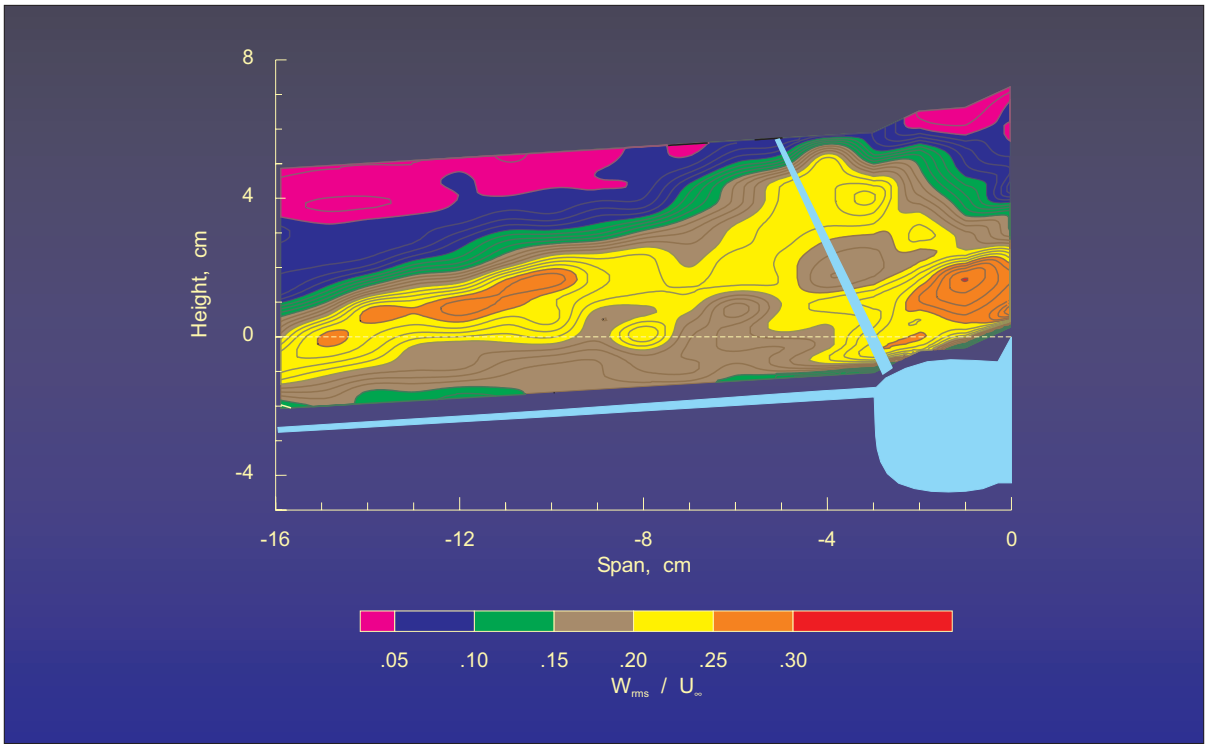

Figure 36.- Contours of traverse normalized standard deviation of the vortex flow above the YF-17 model at an angle-of-attack = 25.0°, station 524.

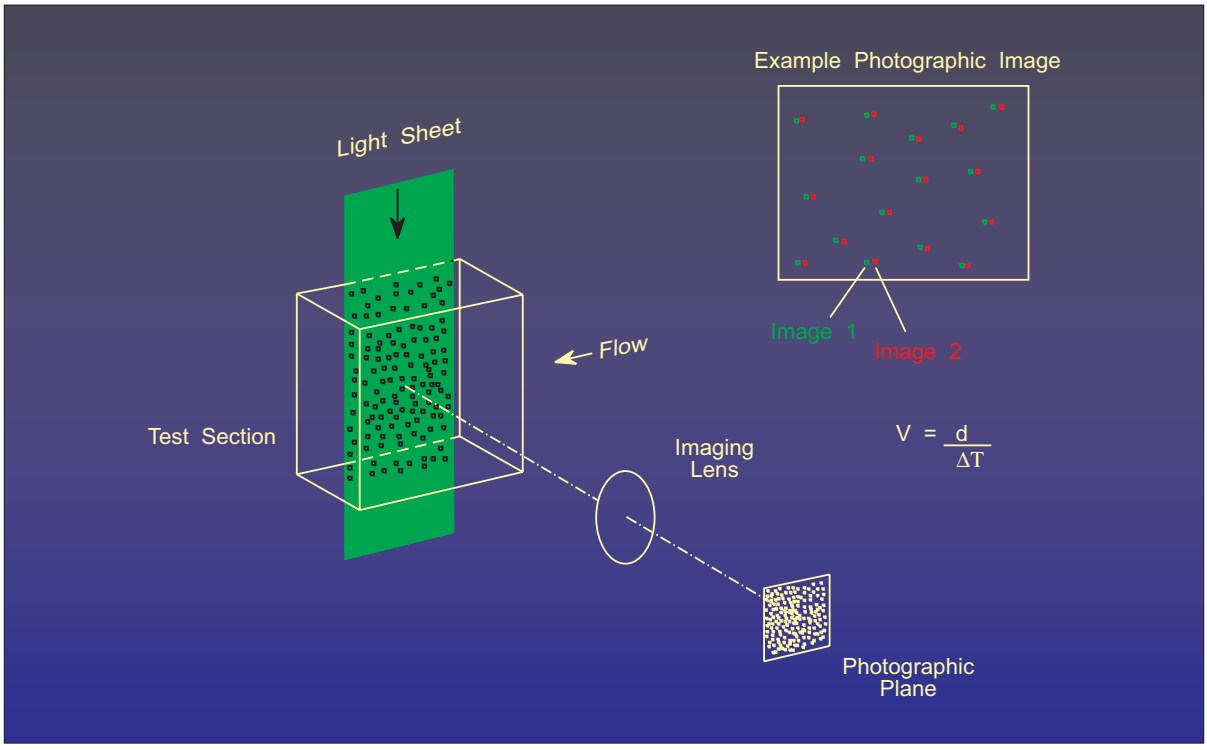

Figure 37.- Diagram illustrating the particle image velocimeter data acquisition optical system.

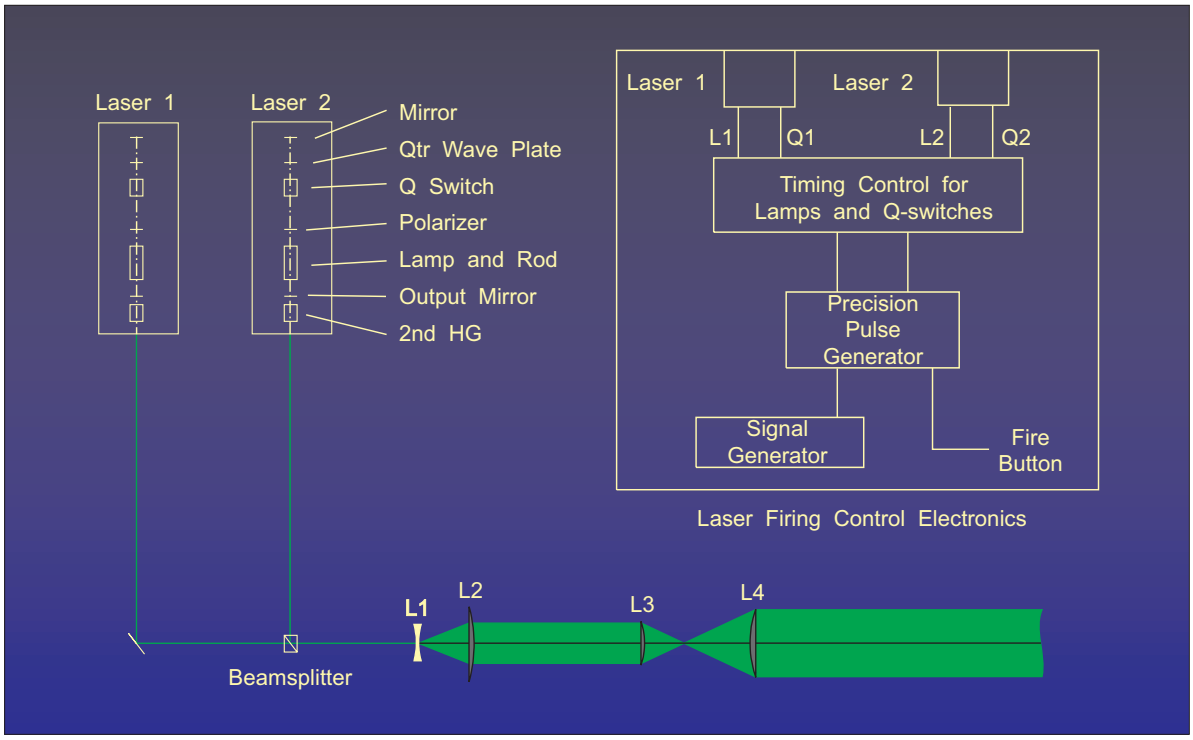

Figure 38.- Diagram illustrating the light sheet generating optical system for the particle image velocimeter.

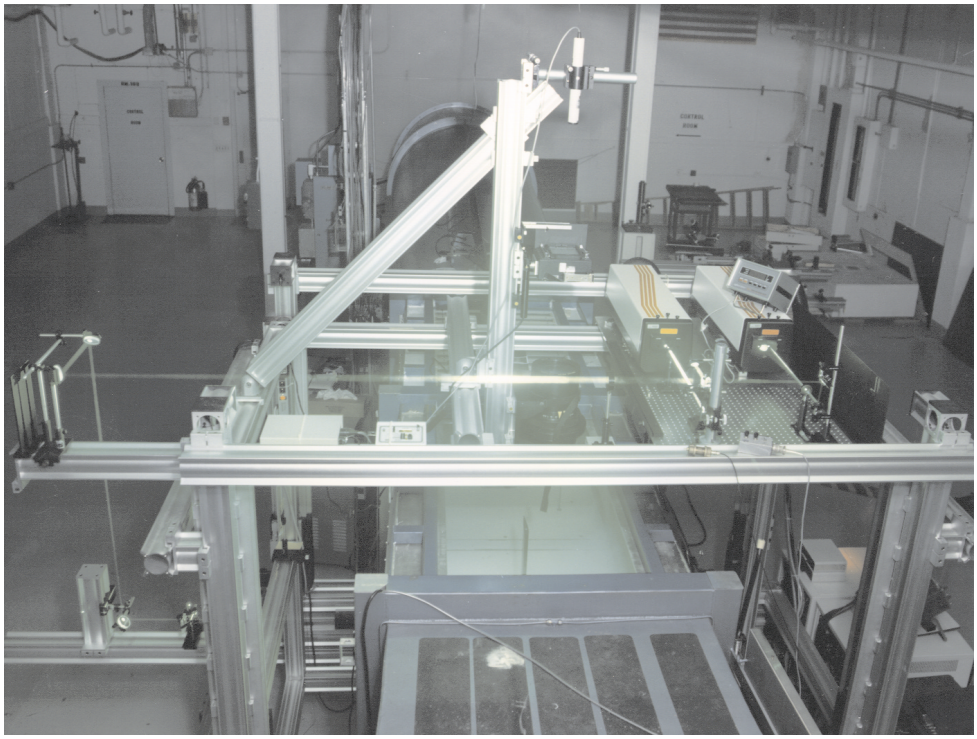

Figure 39.- Photograph of the particle image velocimeter mounted on the laser velocimeter traversing mechanism in the Basic Aerodynamic Research Tunnel.

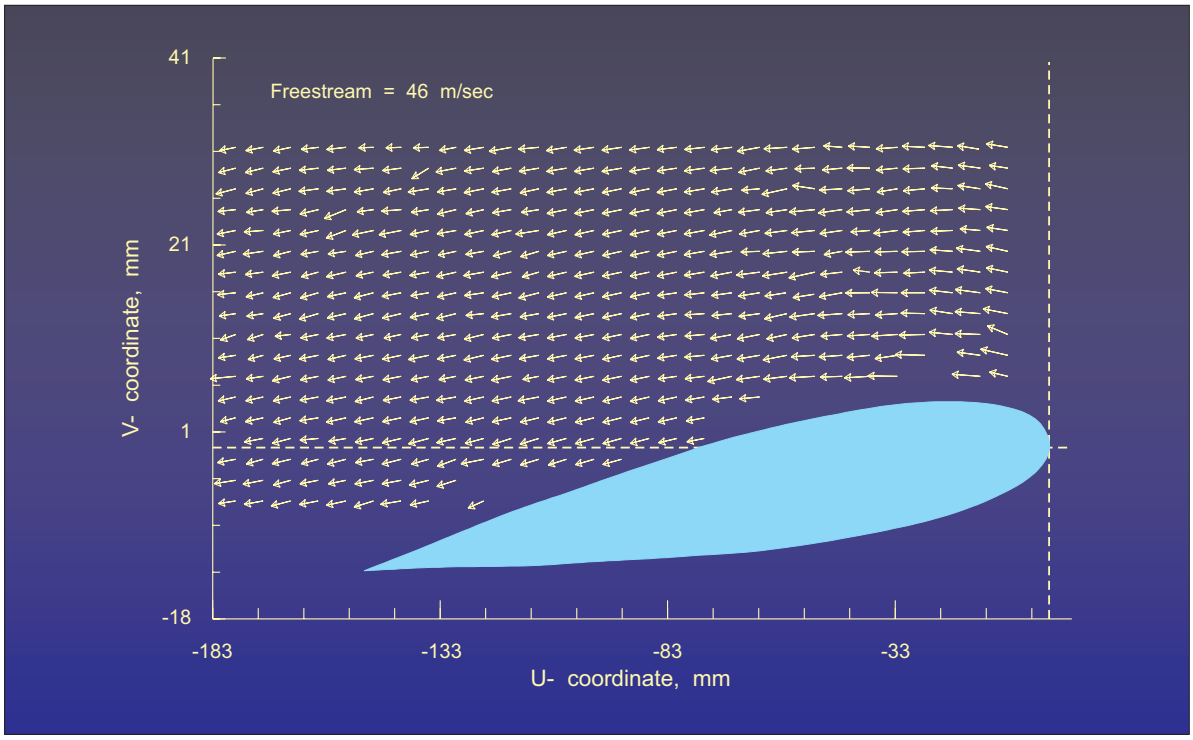

Figure 40.- Mean velocity vectors above a NACA 0012 airfoil measured with the particle image velocimeter using the histogram-based technique for data analysis.

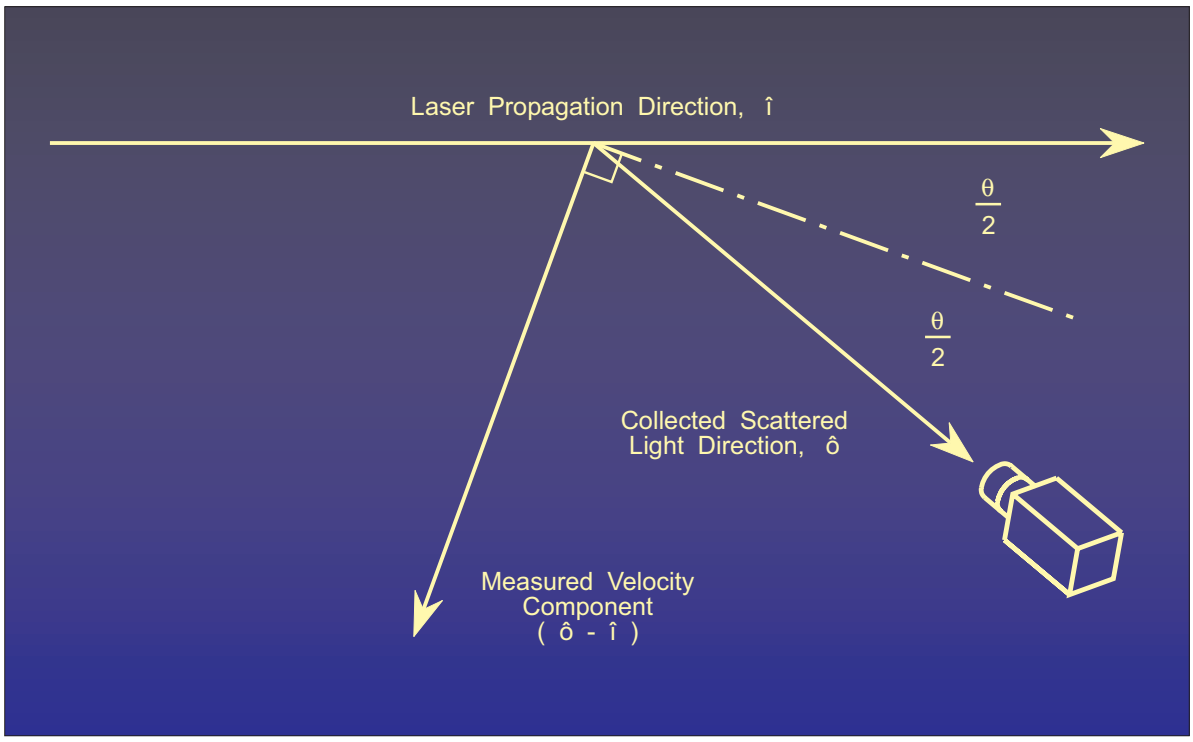

Figure 41.- Determination of measured velocity component direction based on component orientation.

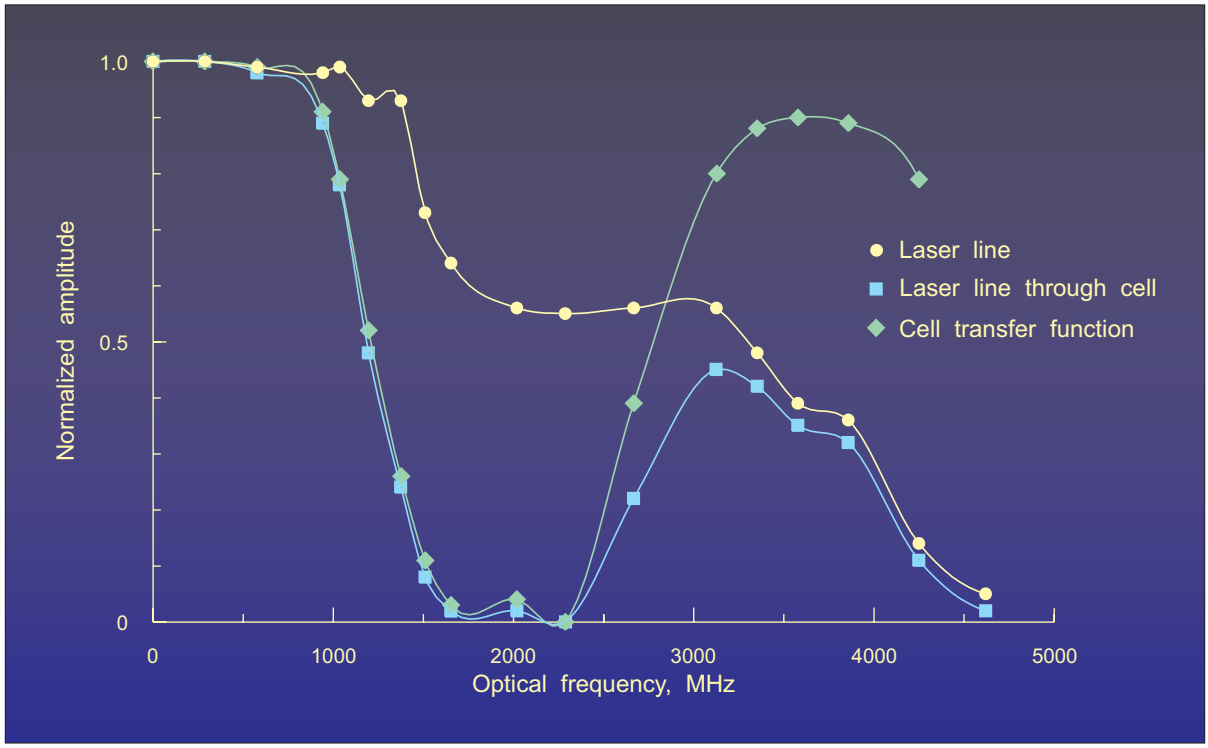

Figure 42.- Transfer function of the Iodine absorption line filter, ALF.

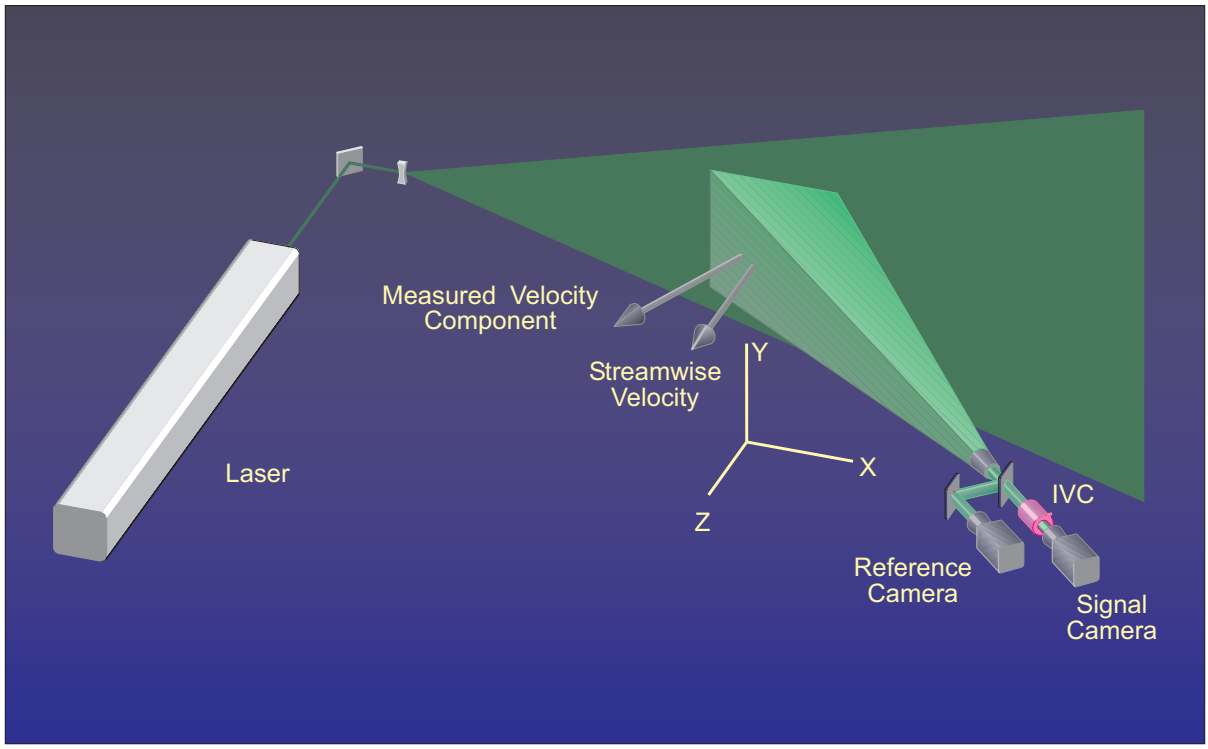

Figure 43.- Graphical representation of the Doppler global velocimeter in the Basic Aerodynamic Research Tunnel, BART.

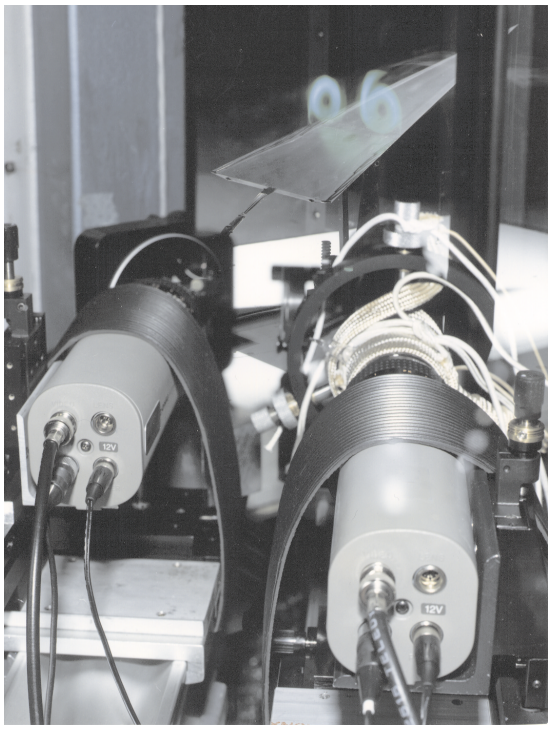

Figure 44.- Photograph overlooking the receiving optical system of the Doppler global velocimeter to view the laser light sheet illuminated vortex flow field above a 75^{o} delta wing.

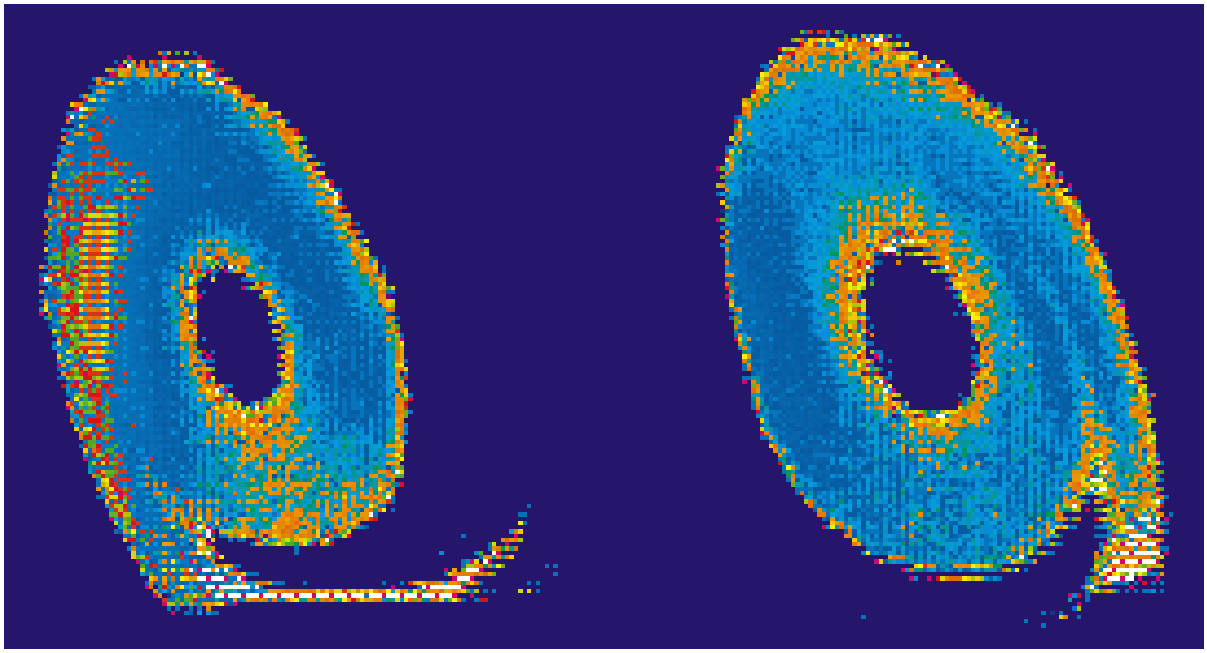

Figure 45.- Single frame DGV velocity contour map of the vortex flow field above a delta wing at 20.5^{o} angle of attack, velocity component is 26.5^{o} from the streamwise direction in the horizontal plane.

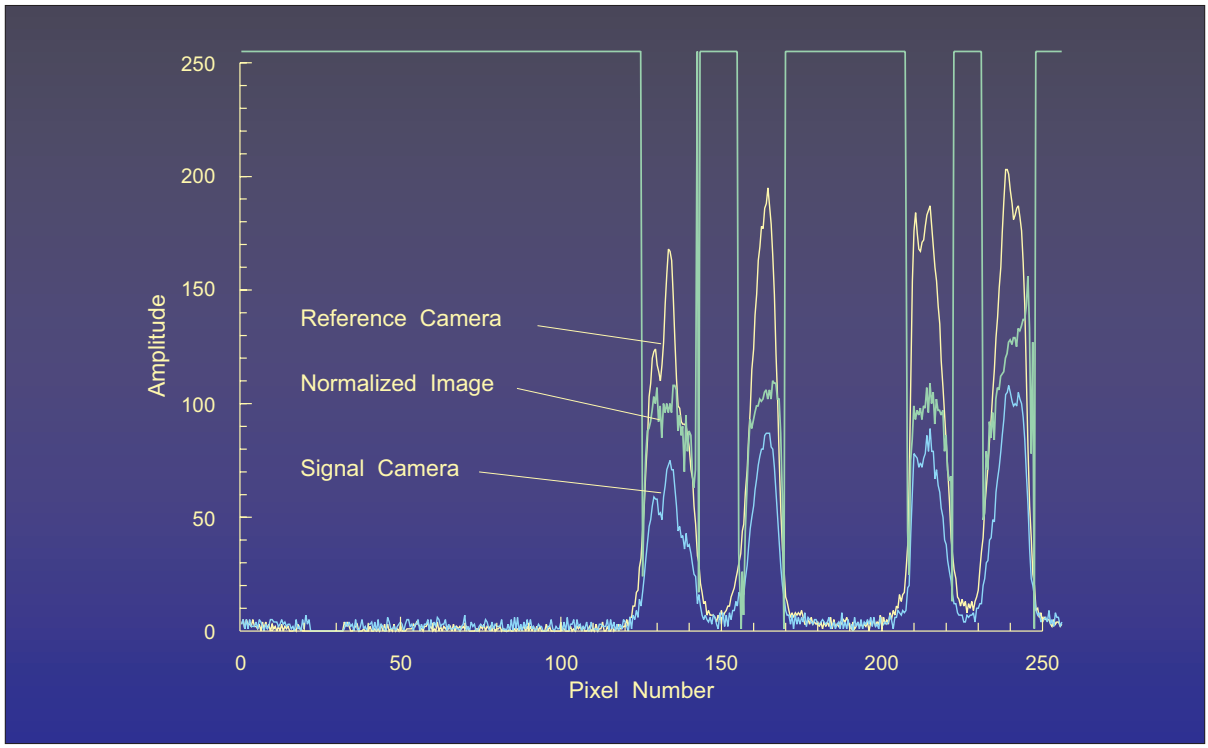

Figure 46.- Signal camera and reference camera signals and the normalized signal along a horizontal line passing through the center of the vortices, (normalized signal amplitude inversely proportional to velocity).